Applied Catalysis B: Environmental 229 (2018) 139–154

Contents lists available at ScienceDirect

Applied Catalysis B: Environmental

journal homepage: www.elsevier.com/locate/apcatb

Mo promoted Ni-Al_2O_3 co-precipitated catalysts for green diesel production

Eleana Kordouli[a,*], Barbara Pawelec[b], Kyriakos Bourikas[c], Christos Kordulis[a,d], Jose Luis G. Fierro[b], Alexis Lycourghiotis[a]

[a] Department of Chemistry, University of Patras, GR-26504, Patras, Greece
[b] Instituto de Catálisis y Petroleoquímica, CSIC, Campus UAM, Cantoblanco, 28049, Madrid, Spain
[c] School of Science and Technology, Hellenic Open University, Tsamadou 13-15, GR-26222, Patras, Greece
[d] Foundation for Research and Technology, Institute of Chemical Engineering Science (FORTH/ICE-HT), Stadiou Str., Platani, P.O. Box 1414, GR-26500, Patras, Greece

ARTICLE INFO

Keywords:
Vegetable oil hydrotreatment
Ni based catalysts
Co-precipitation
Mo promotion
Green diesel

ABSTRACT

Three Mo promoted Ni-Al_2O_3 co-precipitation catalysts with practically the same composition (49–52%wtNi, 6-7%wtMo) were prepared using three different co-precipitation modes: co-precipitation at room temperature using ammonia as precipitating agent as well as co-precipitation at higher temperature (110 °C) using ammonia or urea as precipitating agent. The corresponding un-promoted catalysts were also synthesized for comparison. The catalysts were exhaustively characterized using various techniques and evaluated for the selective deoxygenation (SDO) of natural triglycerides using two different feedstocks: sunflower oil (SO) and waste cooked oil (WCO). The catalytic tests were performed under solvent free conditions in a semi-batch reactor at 310 °C, hydrogen pressure 40 bar and very high reactant volume to catalysts mass ratio (100 mL/1 g).

The promoting action of the Mo(VI) and Mo(IV) well dispersed oxidic phases, was demonstrated in all cases. This was attributed to the impressive decrease in the size of the nickel nanoparticles and to the inhibition of the formation of the catalytically inactive nickel aluminate. Moreover, the Mo (VI) and Mo(IV) oxidic phases affect the network of the SDO favoring the hydrodeoxygenation of the intermediate alcohols with respect to the decarbonylation of intermediate aldehydes.

The catalyst prepared at high co-precipitation temperature using ammonia as precipitating agent was proved to be the most efficient for the SDO of SO. An almost complete transformation of SO into n-C_{15}, n-C_{16}, n-C_{17}, n-C_{18} (green diesel: 97% of liquid products) was obtained under the above mentioned conditions. This catalyst was proved to be very stable. The catalyst prepared at room co-precipitation temperature using ammonia as precipitating agent was proved to be the most efficient for the SDO of WCO (green diesel: 76% of liquid products). Its improved efficiency with respect to the other Mo promoted catalysts was attributed to its smaller pore size which prohibits the blockage of active sites located inside the corresponding pores by bulky compounds present in WCO.

1. Introduction

The transformation of natural triglycerides into hydrocarbons in the range of diesel, namely into the so called “green diesel”, has gained much interest in the last fifteen years [1–4]. This is a promising upgrading alternative compared to the transesterification of natural triglycerides with methanol leading to a mixture of methyl esters of fatty acids, namely to the so called “biodiesel”. Another alternative is the hydrocracking of natural triglycerides resulting to the so called “liquid organic product”, namely to a mixture of hydrocarbons from which green gasoline, kerosene and diesel can be produced by distillation [5–7]. This is usually performed at 400–550 °C and atmospheric pressure over acidic microporous and mesoporous catalysts in the absence or in the presence of small amounts of hydrogen [1,6–8].

Returning to the direct transformation of natural triglycerides into green diesel we are noting that this takes place by selective deoxygenation (SDO) of the natural triglycerides, realized by hydrotreatment in the temperature range of 240–360 °C and hydrogen pressure 10–80 bar over catalysts with moderate acidity. The oxygen removal is proceeding through three parallel pathways, namely direct decarboxylation (deCO_2), decarbonylation (deCO) and hydrodeoxygenation (HDO). The first pathway is more scarce compared to the second and third one. The contribution of deCO and HDO in SDO depends on the catalyst used, temperature and hydrogen pressure. Plant oils are usually used as sources of natural triglycerides.

Two strategies had been emerged from the beginning of the research

* Corresponding author.
E-mail address: ekordouli@upatras.gr (E. Kordouli).

https://doi.org/10.1016/j.apcatb.2018.02.015
Received 6 October 2017; Received in revised form 29 January 2018; Accepted 7 February 2018
Available online 09 February 2018
0926-3373/ © 2018 Elsevier B.V. All rights reserved.

effort in the frame of SDO [1–4]. The so called "combined procedure" in which the plant oil is mixed with gas oil and the mixture is hydrotreated for simultaneous HDS of gas oil and SDO of the plant oil. Adopting this approach the conventional Co (Ni) Mo (W)/γ-Al_2O_3 sulphided catalysts were proved to be effective for both reactions. Following the second approach, called "stand alone", the natural triglycerides are treated separately from petroleum fractions [9–14]. Supported noble metals or the aforementioned sulphided catalysts had been mainly studied from the beginning of the research effort up to 2009. The subject up to this date has been reviewed very successfully by Kubickova and Kubicka [1]. Several problems related to the aforementioned catalysts (limited availability, high cost and sensitivity of the noble metals in oxygenated compounds, requirement for maintaining the Co (Ni) Mo (W)/γ-Al_2O_3 catalysts in their sulphided form by introducing a sulfur containing compound in the feed which presumably leads to an S-contaminated end product) have turned the interest towards the much cheaper nickel based catalysts. A large number of papers have been then published concerning the "non-sulphided nickel based catalysts". The subject was thoroughly reviewed by us in 2016 [2]. Meanwhile, two excellent reviews were reported at 2013 focusing on the SDO reaction mechanism [3,4] and the use of algal oil as future feedstock [3]. These reviews are partly deal with the "non-sulphided nickel based catalysts".

The studies in this particular domain are concerning nickel monometallic catalysts and monometallic nickel phosphide catalysts as well as bimetallic NiMo and NiW catalysts in their reduced, carbide, nitride and phosphide form [2,15–26] Various carriers have been used for supporting the aforementioned active phases (γ-alumina, silica, silica-alumina, titania, various types of zeolites, undoped and doped mesoporous silica, MCM-41, SBA-15, active carbon, carbon nanotubes) [2,27–29]. In almost all cases the supported catalysts were prepared following an impregnation technique, mostly the typical incipient and wet impregnation and in some cases the most sophisticated "equilibrium deposition filtration" (otherwise called "equilibrium adsoption") and the "deposition precipitation". However, the application of one of the aforementioned techniques on a pre-existing support does not frequently result to supported catalysts with high nickel loading keeping at the same time the high value of the specific surface area of the carrier for obtaining as much as higher active surface. Thus, the necessity of using an alternative preparation procedure for obtaining the maximum number of the active sites in a given catalyst mass had been emerged. Co-precipitation is the most convenient method for achieving this goal resulting to low "catalyst to reactor volume" ratio [30,31].

Taking into account the above we recently reported on the preparation of a mesoporous high surface Ni-Al_2O_3 catalyst containing 60 wt% of nickel which is proved to be the best catalyst composition for the transformation of sunflower oil into green diesel [32]. The catalyst was prepared by co-precipitation at room temperature using ammonia as precipitating agent and applying very close control on the preparation parameters. A very high yield of hydrocarbons in the diesel range was obtained under solvent free conditions at 310 °C, hydrogen pressure 40 bar, reactant volume to catalyst mass ratio (100 mL/1 g) and reaction time equal to 9 h using a semi batch reactor. The two latter parameters correspond to a total yield obtained in a fixed bed reactor working at LHSV = 11.1 h^{-1}. This is very high as it is compared to mean value of about 1 h^{-1}, usually reported in the SDO of the natural triglycerides [2]. A complete transformation of triglycerides into hydrocarbons in the diesel range was obtained over the above catalyst for reactant volume to catalyst mass ratio (2 mL/1 g) and reaction time 3 h (corresponding to LHSV = 0.67 h^{-1}) at 260 °C and hydrogen pressure 40 bar [32]. Thus, the application of the co-precipitation method at room temperature using ammonia as precipitating agent was proved very fruitful for preparing very active Ni-Al_2O_3 catalysts. The plausible question had emerged in this point was whether the catalytic performance could further be increased by introducing in the above catalyst formulation a second element acting as promoter. As it will be analyzed in the next paragraph molybdenum seems to be a good candidate [33–36].

The high activity of the conventional Co (Ni) Mo (W)/γ-Al_2O_3 catalysts in their sulphided form and the problems related with the S-contamination of the end product mentioned above motivated research relevant to these catalysts but in their reduced form. It was found that the reduced catalysts are considerably less active than the corresponding sulphided ones [37–39]. The effort for decreasing the difference in the activity was directed quite successfully to the modification of the reduced catalysts with several dopants such as lanthana [37,38], ceria [38] or phosphorus [40–42]. In all these cases, with only one exception [33], it was silently assumed that the synergistic atomic ratio $\frac{Ni}{Ni+Mo} = 0.3$, typical in HDS, is also valid in the SDO of natural triglycerides for the reduced form of the catalysts. This was questioned by us in a very recent article [34]. Working with a series of NiMo/γ-Al_2O_3 reduced catalysts, prepared by incipient wetness impregnation, of varying $\frac{Ni}{Ni+Mo}$ atomic ratio and constant (Mo + Ni) atomic density = 4 atoms/m^2, we have demonstrated that the best ratio was equal to 0.9 for the SDO of the natural triglycerides of sunflower oil. More importantly, an impressive increase of hydrocarbons yield in the diesel range by a factor of 4.77 was achieved by the simple change of the aforementioned ratio from 0.3 to 0.9. However, even at this synergistic ratio the reduced NiMo/γ-Al_2O_3 catalyst with 10 wt% total metal loading (Ni + Mo) remained less active than the Ni-Al_2O_3 catalyst with 60 wt% nickel loading, mentioned in the previous paragraph.

Taking into account the findings described in the two previous paragraphs [32,34] and very recent encouraging results concerning the Mo promoting action on nickel catalysts supported on γ-alumina for the transformation of methyl laurate to hydrocarbons [35] it appeared to us interesting to develop a Mo promoted Ni-Al_2O_3 co-precipitation catalyst with total nickel and molybdenum loading equal to 60 wt% by taking into advantage both the best optimum loading in the active element [32] and the optimum $\frac{Ni}{Ni+Mo}$ atomic ratio [34] as well. More precisely, in the present work we are preparing three Mo promoted Ni-Al_2O_3 co-precipitation catalysts with practically the same composition using three different co- precipitation modes: co-precipitation at room temperature using ammonia as precipitating agent (MoNiAar) as well as co-precipitation at higher temperature using ammonia (MoNiAah) or urea (MoNiAuh) as precipitating agent. The corresponding un-promoted catalysts were also synthesized for comparison (NiAar, NiAah and NiAuh).

The catalysts were characterized using various techniques and evaluated for the SDO of natural triglycerides using two different feed stokes: sunflower oil (SO) and waste cooked oil (WCO). SO was chosen for the following reasons: (a) it is already used as a raw material for producing biodiesel, (b) although SO is an edible oil, genetically modified sunflower grown on marginal land (e.g. old mining lands, irrigation canals) has been recognized as a sustainable biofuel source because it does not demand arable lands [43], (c) the sunflower seeds contain quite high amounts of oil. The use of WCO, on the other hand, was based on the following reasons: (a) WCO is also used to produce biodiesel, (b) the collection of WCO, imposed by the environmental legislation, provides, in effect, a very cheap and actually renewable raw material, (c) large quantities of WCO are available throughout the world (~100 million gallons/d are produced in USA) [44]. Taken into account the above and that the production of green diesel is economically favorable or of equal cost compared to the production of biodiesel [45–47], one may expect that SO and WCO would be used in the near future for producing green diesel.

2. Experimental

2.1. Feedstocks

The SO used in the present study was purchased from the food market. The natural triglycerides of the SO have side chains

corresponding to about eleven fatty acids in the range of 16–20 carbon atoms. Most side chains correspond to linoleic (71.7%), oleic (15.9%), palmitic (5.8%) and stearic acid (3.9%). The WCO was obtained by the "Collectoil" company. It was filtered three times using cloth filters of different sizes. Then it was centrifuged prior to its use. Feedstock characteristics (density, viscosity, acidity, iodine number and oligomer content) have been reported elsewhere [34]. It should be stressed that WCO is characterized by higher density, viscosity and acidity than SO and contains 1.5 wt% oligomers.

2.2. Catalysts preparation

As already mentioned six samples of Ni-Al_2O_3 and Mo promoted Ni-Al_2O_3 catalysts were prepared by co-precipitation: (i) at room temperature using NH_4OH aqueous solution as precipitation agent, (ii) at high temperature using the same precipitation agent and (iii) at high temperature using urea aqueous solution as precipitating agent. All the samples contained the same amount of Al_2O_3 (ca. 40 wt %). In the bimetallic catalysts the $\frac{Ni}{Ni+Mo}$ atomic ratio was ≈0.9. The symbols of the samples have been mentioned previously.

2.2.1. Co-precipitation at room temperature

Carefully weighted amounts of $Ni(NO_3)_2.6H_2O$ (Merck, kGaA), $Al(NO_3)_3.9H_2O$ (Alfa Aesar) and $(NH_4)_6Mo_7O_{24}$ $4H_2O$ (Alfa Aesar) in the case of bimetallic catalyst were dissolved in distilled water. This solution was fed by a syringe pump to a beaker containing NH_4OH aqueous solution with pH = 8. The pH in the beaker was maintained constant during preparation using a pH-stat (Metrohom-645, iso-Dosimat) which fed concentrated NH_4OH aqueous solution (25–28% PENTA). A suspension of hydroxides ($Ni(OH)_2$-$Al(OH)_3$ containing Mo-oxo species in the case of Mo-promoted sample) was produced. This was vacuum-filtered and the solid obtained was washed with 3-distilled water and was dried at 110 °C in air overnight.

2.2.2. Co-precipitation at high temperature using NH_4OH aqueous solution as precipitation agent

The aforementioned salts were dissolved in concentrated NH_4OH aqueous solution in a spherical flask with reflux condenser and magnetic stirrer immersed in a heated oil bath (110 °C). After 6 h the suspension obtained was cooled down to ambient temperature and was filtered. The solid obtained was washed with 3-distilled water and dried at 110 °C overnight.

2.2.3. Co-precipitation at high temperature using urea aqueous solution as precipitation agent [48]

The precursor salts were dissolved in water in a spherical flask. A $CO(NH_2)_2$ aqueous solution was added (Duchefa) containing the triple amount of urea molecules with respect to the NO_3^- radicals of the precursor salts. A reflux condenser and magnetic stirrer were installed and the system was immersed in a heated oil bath (110 °C). After 10 h the suspension obtained was cooled down to ambient temperature and filtered. The solid was washed with 3-distilled water and dried at 110 °C overnight.

The hydroxides in the dried samples were decomposed to the corresponding oxides under Ar (30 mL/ min) in a fixed bed quartz reactor by increasing the temperature (5 °C/min) from room temperature up to 400 °C remaining there for 1 h. This procedure leads to the formation of the catalyst precursors. The final catalysts were obtained by reduction of the catalyst precursors at 400 °C for 2.5 h in a stream of H_2 (30 mL/min). One of the samples was reduced at various temperatures in the range 400–550 °C. The activation of each sample was ended by its passivation feeding the reactor at room temperature with 1 v/v% O_2 in Ar stream (20 mL/min) for 0.5 h.

2.3. Catalysts characterization and evaluation

The nickel and molybdenum loading of the prepared catalysts was calculated by subtracting their amount remaining in the aqueous phase (filtrates) after co-precipitation from that initially used. The metal concentrations of the filtrates were determined spectrophotometrically. More precisely, dimethylglyoxime (DMG) was added to the filtrates and a soluble anionic complex with the formula $Ni(DMG)_2^{2-}$ was obtained. Its concentration was determined at 445 nm [49]. Total Mo content of filtrates was determined at 490 nm [50]. UV–vis spectrophotometer (Varian Cary 3) was used for these measurements.

The composition results obtained were confirmed by EDS analysis of the final catalysts performed on a Scanning Electron Microscope (SEMJEOL JSM6300) equipped with an Energy Dispersive Spectrometry accessory. The chemical composition of the samples was determined using natural and synthetic standards and 20 kV accelerating voltage with 10 nA beam current. Microanalysis was performed on gold coated samples. The sample powders were mounted directly on the sample holder. The morphology of the samples was also examined using the same microscope.

X-ray diffraction patterns were used for investigating the crystal structure of the samples. These were recorded in a BruckerD8 Advance diffractometer equipped with nickel-filtered CuKα (1.5418 Å) radiation source. The step size and the time per step were respectively fixed at 0.02° and 0.5 s in the range of $10° \leq 2\theta \leq 80°$.

The transmission electron microscopy analysis of the samples was conducted on a JEOL JEM-2100 system operated at 200 kV. TEM images were recorded using an Erlangshen CCD Camera (Gatan Model 782 ES500W), while Kodak SO-163 films were used for HRTEM images. The specimens were prepared by dispersion in water and spread onto a carbon-coated copper grid (200 meshes).

Raman spectra were recorded with a Renishaw in Via Raman Microscope spectrometer equipped with a laser beam emitting at 785 nm, at 310 mW output power. The photons scattered by the sample were dispersed by a 1200 lines/mm grating monochromator and simultaneously collected on a CCD camera; the collection optic was set at 50× objective.

The BET specific surface area and the BJH pore size distributions of the samples were determined from the nitrogen adsorption–desorption isotherms recorded using a Micromeritics apparatus (Tristar 3000 porosimeter) and the corresponding soft-ware.

H_2-TPR experiments were performed in laboratory-constructed equipment described elsewhere [51]. An amount of sample, 0.04 g, was placed in a quartz reactor and the reducing gas mixture (H2/Ar: 5/95 v/v) was passed through it for 2 h with a flow rate of 40 ml min^{-1} at room temperature. Then the temperature was increased to 1000 °C with a constant rate of 10 °C min^{-1}. Reduction leads to a decrease of the hydrogen concentration of the gas mixture, which was detected by a thermal conductivity detector (TCD) (Shimadzu). The reducing gas mixture was dried in a cold trap (−95 °C) before reaching the TCD.

NH_3-TPD experiments were performed in the aforementioned laboratory-constructed equipment. In a typical experiment, 100 mg of the pre-reduced catalyst were placed in a quartz microreactor. The sample was heated under He flow (30 cm^3 min^{-1}) at 450 °C for 15 min to remove adsorbed species from the catalyst surface and then cooled down to room temperature. Next, a stream of NH_3/He was introduced in the reactor for 30 min at room temperature, and then switched to He to remove physically adsorbed ammonia. The temperature was then increased linearly up to 500 °C at a rate of 15 °C/min. An Omnistar/Pfeiffer Vacuum mass spectrometer (MS) was used for on-line monitoring of effluent gas. NH_3 response signal of the mass spectrometer was calibrated against a standard mixture of accurately known composition.

The X-ray photoelectron spectra of in situ reduced catalysts were recorded on a VG Escalab 200R electron spectrometer equipped with a hemispherical electron analyzer, using a MgKα ($h\nu$ = 1253.6 eV,

1 eV = 1.603 × 10^{-19} J) X-ray source operated at 10 mA and 12 kV. The ECLIPSE software was used to record and analyze spectra. The line of C 1s at 284.8 eV (accuracy within ± 0.1 eV) was used as an internal standard to correlate the values of the binding energy obtained in order to normalize the charging effects appearing commonly on non-conductive samples. Each spectral region of the photoelectrons of interest was scanned a number of times to obtain a good signal-to-noise ratio. The intensity of the peaks was estimated by calculating the integral of each peak after subtraction of background and by fitting the experimental peak to a combination of Lorentzian/Gaussian lines of variable proportions.

A falling basket batch reactor (300 mL, Autoclave Engineers) working in a semi-batch mode was used for evaluating the catalysts at 310 °C, 40 bar hydrogen pressure and reactant volume to catalyst mass ratio equal to 100 mL/1 g. An amount (1 g) of activated catalyst was added to the reactor basket being maintained at its upper position. After that the reactor was purged three times with Ar prior to be pressurized with H_2 (40 bar). The hydrogen flow rate was controlled to 100 ml/min by a flow controller (Brooks 58505S) and the speed of stirring to 1000 rpm. The reactor was heated with a temperature rate 10 °C/min to the reaction temperature (310 °C). Then the basket was falling into the liquid phase. This was the starting point of the reaction. A liquid sample of 2 ml was withdrawn from the reactor every hour and analyzed by gas chromatography using a Shimadzu GC-2010 plus gas chromatograph equipped with a flame ionization detector (FID) and an appropriate column (SUPELCO, MET-Biodiesel, l = 14 m, d = 0.53 mm, tf = 0.16 μm). Gas-phase analysis was performed on line for selected experiments. The gas composition was determined using a six-port sampling valve and a Shimadzu GC-8A chromatograph equipped with a thermal conductivity detector and an appropriate column (SUPELCO, 110/120 Carbosieve S II, 10F, 1/8 in). The reaction was monitored for a period of 9 h.

3. Results and discussion

3.1. Catalysts characterization

3.1.1. Morphology and texture

Table 1 illustrates the catalysts prepared, their composition obtained by EDS and textural characteristics. Inspection of this table shows that the chemical compositions of the catalysts determined by EDS are actually very close to the corresponding nominal ones. Moreover, these are almost identical to the corresponding ones determined by spectroscopic analysis of nickel and molybdenum in the solution resulting after the filtration which follows the co-precipitation procedure. An almost constant composition was determined at different places of a SEM image indicating uniform distribution at micro scale. The values of atomic ratio $\frac{Ni}{Ni+Mo}$ obtained for the Mo promoted samples are about 0.9, equal to the optimum reported in our previous work [34].

Fig. 1 illustrates the SEM images recorded at quite high magnifications for the samples studied. Inspection of this figure shows that the morphology of the samples at nanoscale depends strongly on the preparation temperature. Both samples prepared at room temperature exhibit granular morphology indicating that the presence of molybdenum phases does not actually disturb the shape of the catalyst agglomerates. The increase of the preparation temperature changes dramatically the morphology from granular into “flower” one. In that case agglomerates with nano-flake structure constitute flower like assemblies. We are noting that this structure does not depend on the presence of molybdenum species or the substance used as precipitating agent.

The formation of hierarchical NiO flake-flower architectures following a hydrothermal precipitation procedure in the presence or absence of a surfactant and using ammonia or urea as precipitating agents has been reported several times in the last years [52–55]. This is because NiO is a significant p-type semiconductor with applications in catalysis, electro-catalysis, lithium ion batteries, magnetic materials and gas sensors. Although the mechanistic routes proposed by the various groups differ in details, a rather widely accepted mechanism involves the formation of $Ni(OH)_2$ nuclei by homogeneous-spontaneous precipitation followed by crystal growth and random aggregation of the crystals resulting first to a rather granular morphology (First step). As the process is progressed the adjacent crystals/small particles are re-aggregated forming nanoflakes via a spontaneous self–organization of these entities (Second step). As the process time increases further the nanoflakes begins to pile up resulting to nano-flower architectures (Third step). The formation these architectures can be related to the layered double hydroxide structure of $Ni(OH)_2$ and to the relatively high precipitation temperature which accelerates the second and the third step of the whole procedure. It is worth note that the heating of the precipitated $Ni(OH)_2$ in air transform it to NiO without disturbing the nano-flower architectures [52–54].

Taking into account the above we may easily attribute the NiO like flake-flower architectures obtained in the samples NiAah, NiAuh, MoNiAah and MoNiAuh (Fig. 1) to their high nickel content. It seems that the activation by reduction as well as and the presence of amorphous alumina and the well dispersed Mo(iv) and Mo(vi) oxo-phases (see below) do not disturb the nano-flower architectures dictated by the initially formed $Ni(OH)_2$. The achievement of these architectures can be attributed to the relatively high co-precipitation temperature (110 °C) and to relatively high precipitation time (6 h for the samples NiAah, and MoNiAah and 10 h for the samples NiAuh and MoNiAuh). On the other hand, the relatively low co-precitation time (4 h) and the relatively low temperature (room temperature) which is not sufficient for the acceleration of the second and third step of the aforementioned co-precipitation mechanism resulted to granular morphology observed in NiAar and MoNiAar samples (Fig. 1).

Going from morphology to the texture of the catalysts studied we are noting that a quite high specific surface area is obtained in all cases (Table 1). The samples are exhibiting a mesoporous-small macroporous texture. This is reflected in the form of the isotherms and the hysteresis loops as well (Fig. 2).

The type H3 of the hysteresis loops indicates the formation of aggregates of plate like-particles forming slit-like pores. The appearance of the loops at lower p/p° values in the samples NiAar and MoNiAar

Table 1
Catalysts, composition obtained by EDS, textural characteristics [specific surface area (SSA), specific pore volume (SPV), mean pore diameter (MPD)], mean crystal size of Ni° calculated by Scherrer's equation (D_{NiXRD}), and weak to medium strength acid sites population $(W/M)_{TPD}$ calculated from NH_3-TPD curves.

Catalyst	Ni_{EDS} (wt%)	Mo_{EDS} (wt%)	$(\frac{Ni}{Ni+Mo})_{EDS}$	SSA (m^2/g)	SPV (cm^3/g)	MPD (nm)	D_{NiXRD}(nm)	$(\frac{W}{M})_{TPD}$
NiAar	57.78	–	–	272	0.59	6.7	8.9	3.2
NiAah	60.00	–	–	159	0.49	12.0	11.7	3.2
NiAuh	59.00	–	–	164	0.50	10.1	8.1	2.6
MoNiAar	49.90	6.91	0.92	262	0.55	6.8	7.0	3.8
MoNiAah	50.80	5.78	0.93	219	0.53	9.4	6.6	3.3
MoNiAuh	51.30	6.02	0.93	229	0.54	7.8	7.6	2.5

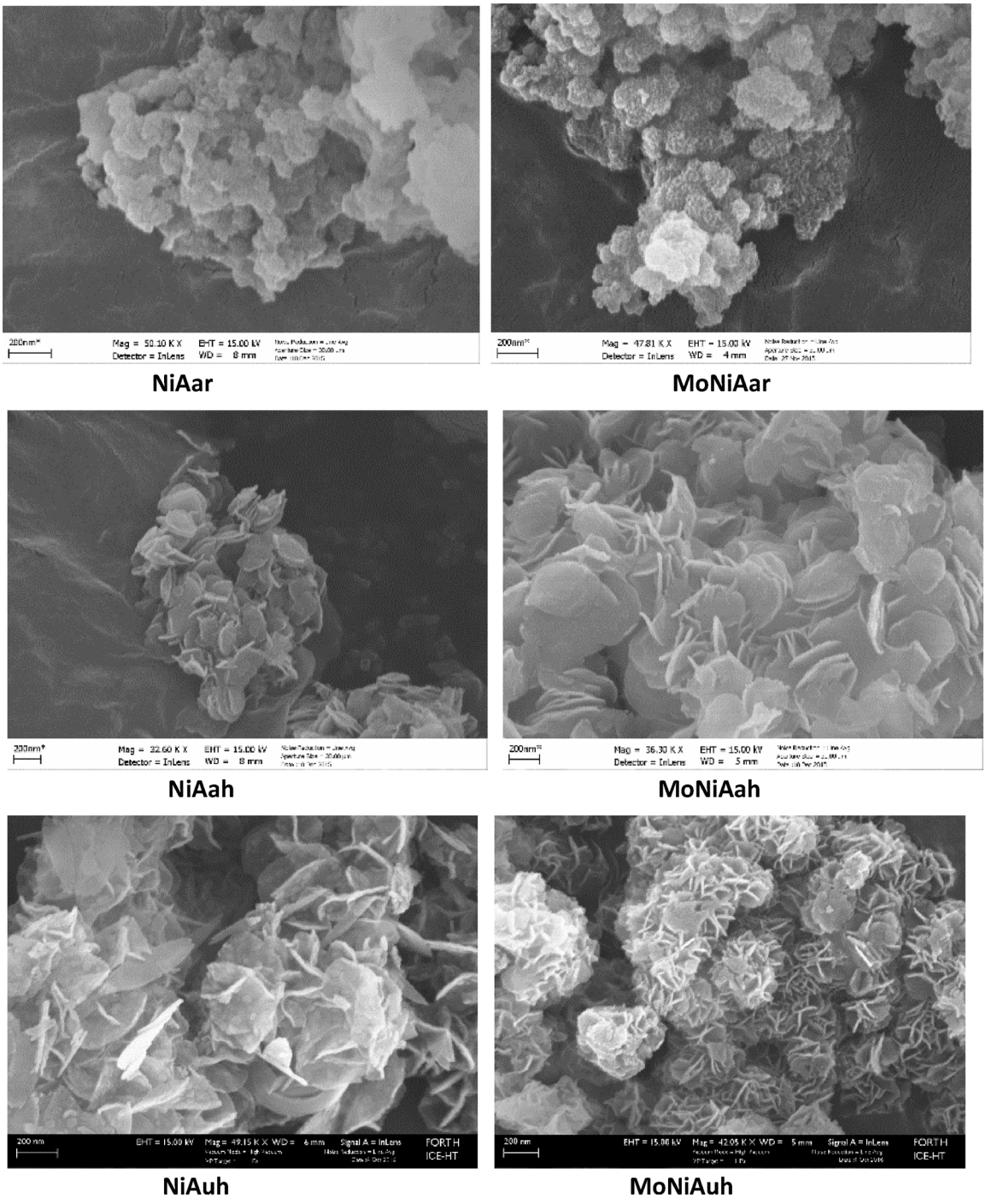

Fig. 1. SEM images recorded for the NiA and MoNiA catalysts prepared by co-precipitation using NH_3 at room (ar) or high (ah) temperature and urea at high temperature (uh).

with respect to the other samples indicates a preference for quite small mesopores in these samples. This is indeed the case as one may see in Fig. 3 which illustrates the pore volume distribution of the samples studied. In fact, the increase of the co-precipitation temperature decreases significantly the pore volume fraction of the small pores for both the promoted and the un-promoted samples. Moreover, inspection of this figure confirms the mesoporous-small macro-porous texture of the catalysts studied with mean pore diameters and specific pore volumes in the range 6.7–12.0 nm and 0.49–0.59 cm^3/g, respectively (Table1).

The specific surface areas of the promoted catalysts prepared at high temperature are considerable higher than the corresponding un-promoted ones. The high specific surface area determined for the samples NiAar and MoNiAar (Table 1) can be attributed to the relatively large pore volume of the mesopores in these samples (Fig. 3). Concerning the Mo-promoted samples the increase in the co-precipitation temperature increases the pore volume of the macro-pores range (Fig. 3).

3.1.2. Structure and dispersion of the nickel and molybdenum phases

The crystal structure of the catalysts studied was first investigated by XRD. The XRD patterns are illustrated in Fig. 4. In all these patterns the peaks appearing indicate the formation of metallic Ni (44.58, 51.80 and 76.31°, JCPDS04-0850), NiO (43.30, 37.27 and 62.82°, JCPDS22–1189) and $NiAl_2O_4$ (37.03, 45.02 and 65.37°, JCPDS 10-0339) crystals. Peaks relevant to the presence of Al_2O_3 are not present in the XRD patterns indicating the formation of amorphous alumina.

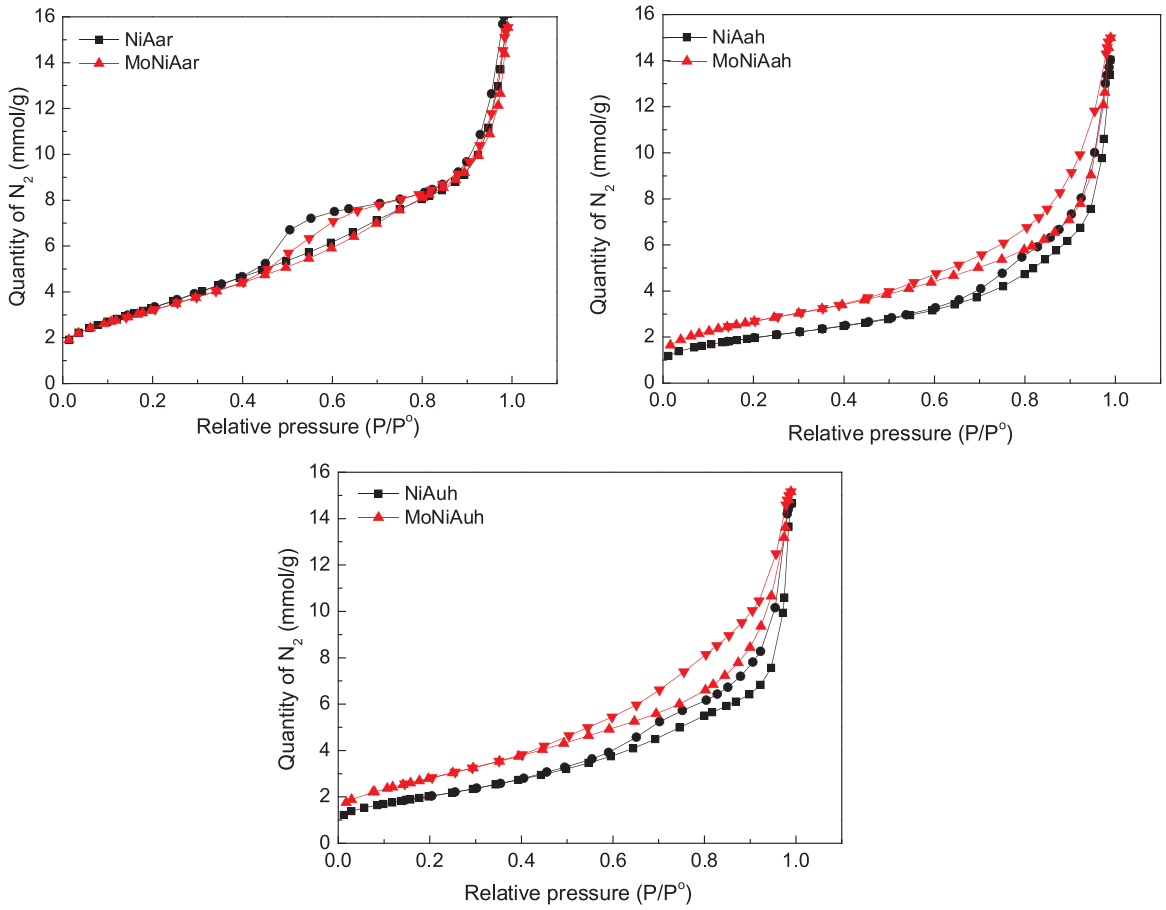

Fig. 2. Adsorption-Desorption isotherms of the NiA and MoNiA samples prepared by co-precipitation using NH_3 at room (ar) or high (ah) temperature and urea at high temperature (uh).

The absence of peaks relevant to crystal phases of Mo species presumably indicates their very good dispersion or the formation of amorphous Mo phases.

Concentrating our attention on the peaks at $2\theta = 51.80^\circ$ and $2\theta = 76.31^\circ$ attributed exclusively to the metallic nickel (Ni°) we are noting that the presence of the molybdenum phases renders these peaks much less acute indicating the decrease in the size of the corresponding crystals. This is indeed the case (Table 1).

It is remarkable that this important effect of the molybdenum species is independent of the co-precipitation mode applied for the preparation of the catalysts. Concentrating our attention to the peaks at $2\theta = 44.58^\circ$ and 43.3° we are seeing that in all cases the presence of molybdenum species favors the formation of nickel oxide with respect to the metallic nickel. The above two effects are presumably interrelated. During the activation of the samples the nickel hydroxide initially formed in the precipitation step is transformed into nickel oxide by dehydration upon heating in argon atmosphere and then it is reduced to metallic nickel upon activation in hydrogen stream. The ability of the molybdenum species to disperse the nickel phases leads to the formation of relatively small nickel oxide nanocrystals strongly interacted with the alumina surface and thus more resistant to the reduction. Finally, the presence of the molybdenum species also affects the relative amounts of the NiO and $NiAl_2O_4$ as it can be inferred from the relative intensities of the peaks at 62.82 and 65.37°, respectively. In the samples prepared at room (high) temperature the presence of molybdenum species increases (decreases) the relative amount of the $NiAl_2O_4$ crystal phase.

The electron diffraction patterns of the samples studied, taken in the frame of the application of the TEM technique (not presented here), showed the presence of the aforementioned nickel phases, principally of metallic nickel and nickel oxide, and the absence of alumina and molybdenum crystal phases, in full agreement to the XRD results. The crystal planes of the metallic nickel (2 0 0 and 2 2 0) and nickel oxide (1 1 1) were also detected in the HRTEM images. A representative image is illustrated in Fig. 5.

Moreover, the TEM images (Fig. 6) of the samples studied visualize much better the increase in the dispersion of the nickel phases due to the presence of the molybdenum species. This is because the XRD patterns are sensitive only to nanocrystals larger than 4 nm. The decrease in the size of the nickel/nickel oxide nanocrystals from 5–20 to 2–4 nm determined by TEM images is indeed impressive.

The increase in the dispersion of the nickel phases deduced by XRD and TEM is also confirmed by the XPS results. These results provide, moreover, useful information concerning the molybdenum phases formed. Fig. 7 illustrates, as an example, the XPS spectra of the samples NiAar and MoNiAar. Very similar spectra were obtained for the other samples.

Inspection of Fig. 7 shows the presence of Ni° and the $Ni^{2+\cdot}$ on the surfaces of studied samples. The latter is due to the formation of NiO and $NiAl_2O_4$. This is in full agreement to the XRD, TEM and HRTEM results. The XPS spectra indicate, moreover, the presence of two molybdenum oxidic species, namely Mo(VI) oxo-species and Mo(IV) oxo-species, well dispersed and thus not detectable by XRD.

Critical XPS parameters calculated using the XPS spectra are illustrated in Table 2. In all cases the amount of the Mo(VI) oxo-species is considerably higher than that of Mo(IV) ones (Table 2, 2nd column). The examination of the Ni to Al atomic ratio values, $(Ni/Al)_{at}$ (Table 2, 5th column), which express the dispersion of the nickel phases, confirms the XRD and TEM findings that the presence of the molybdenum oxo-species increases considerably the dispersion of the nickel phases. The most important effect is observed for the sample MoNiAah in which it is observed the maximum dispersion of the molybdenum oxo-species

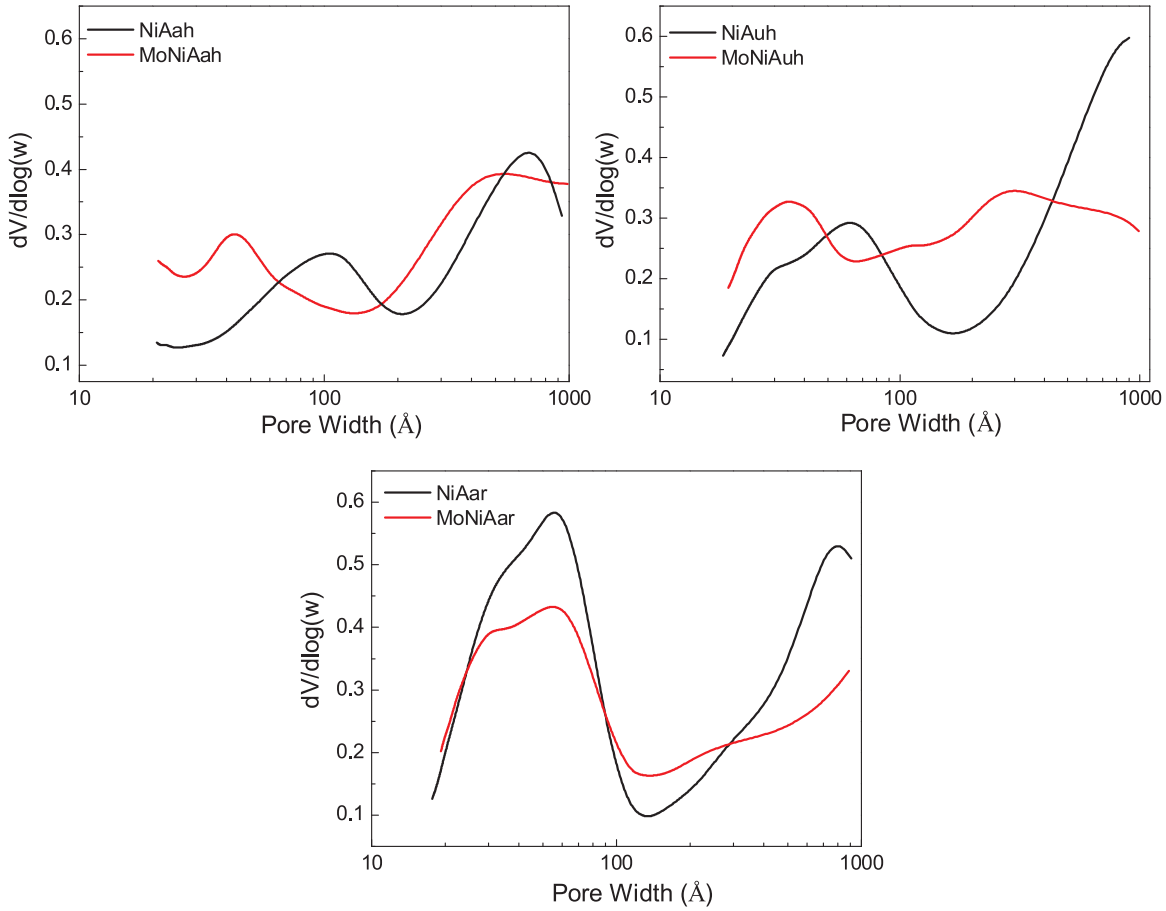

Fig. 3. Pore size distributions obtained for the NiA and MoNiA catalysts prepared by co-precipitation using NH_3 at room (ar) or high (ah) temperature and urea at high temperature (uh).

as well $((Mo/Al)_{at}$ values, Table 2, 4th column). This evidences that the dispersion of the Mo oxides dictates the dispersion of the nickel phases.

The XPS data show also that the presence of the molybdenum oxo-species favors the formation of Ni^{2+} with respect to Ni0 (Table 2, 3rd column). This perhaps means that the molybdenum oxo-species favor nickel oxide with respect to metallic nickel, in agreement to the XRD. Such a stabilization action of Mo oxo-species on NiO phase could be attributed to an interaction between the Ni^{2+} ions and Mo oxo-species developed upon co-precipitation process. However, as it is not easy to quantify the amounts of NiO and $NiAl_2O_4$ phase on the basis of the above spectra this point will be further investigated by H_2-TPR.

The comparison of the $\frac{Ni}{Ni+Mo}$ atomic ratio values obtained by XPS (Table 2, 6th column) with the corresponding bulk ones (Table 1) does not show considerable differences suggesting almost uniform micro distributions of the molybdenum and nickel phases in the catalysts nanoparticles.

The formation of very well dispersed Mo oxo-species inferred by the XRD and TEM and detected by XPS was also confirmed by Raman spectroscopy. Fig. 8 illustrates the Raman spectra of the sample MoNiAah, taken as an example, at each step of the preparation procedure (after drying, heating in argon and heating in hydrogenation atmosphere) together with the spectrum of bulk-crystalline MoO_3. The most important observation is that bands expected for crystalline MoO_3 nanoparticles (663, 821 and 996 cm^{-1}) [56–58] are not detected in the Raman spectra of the sample MoNiAah at any step of the preparation procedure. The spectrum of the sample MoNiAah after drying presents a band at 1045 cm^{-1} assigned to NO_3^- ions [59]. This disappears after the decomposition step taking place upon heating the sample in argon atmosphere. The band at 904 cm^{-1} is due to the MoO_4^{2-} species in tetrahedral coordination [60] present from the early preparation step. This band appears at 854 cm^{-1} in the Raman spectra recorded after the decomposition and reduction steps indicating that monomeric Mo oxo-species are also present in the final catalyst. The above clearly show that the precipitation in very alkaline solution causes the depolymerization of $Mo_7O_{24}^{6-}$ ions of the salt used as Mo source and the formation Mo monomeric species well dispersed on alumina [61]. The XPS spectra showed that these well dispersed Mo(VI) oxo-species are partly reduced upon the activation step resulting to well dispersed Mo(IV) oxo-species.

3.1.3. Reducibility and surface acidity

The H_2-TPR profiles of the samples studied are seen in Fig. 9. First, we are noting that these profiles were recorded after heating at 400 °C in argon atmosphere following the co-precipitation and drying steps. Therefore, the hydroxides formed in the co-precipitation step are expected to be decomposed into oxides. The H_2-TPR curves obtained over all samples can be deconvoluted into three peaks. The first two peaks are assigned to the reduction of NiO into metallic nickel and the third to the reduction of $NiAl_2O_4$ [62]. A contribution in the H_2-TPR curves of the Mo(VI) → Mo(IV) reduction [63] inferred by XPS (Table 2) cannot be excluded but it is expected to be quite small due to the relatively small amount of the Mo-oxo species contained in the samples.

The low temperature reduction peak is attributed to the reduction of NiO with rather low dispersion and weak interaction with the alumina surface. It seems that the increase in the preparation temperature increases the dispersion (in agreement with XPS results, Table 2) and strengthens the interaction of the NiO species with the alumina surface as the reduction peak appears at 298, 417 and 422 °C in the samples NiAar, NiAah and NiAuh, respectively.

The presence of the well dispersed Mo(VI) and Mo(IV) oxo-species increases considerably the reduction temperature and decreases significantly the magnitude of low temperature peak in all cases.

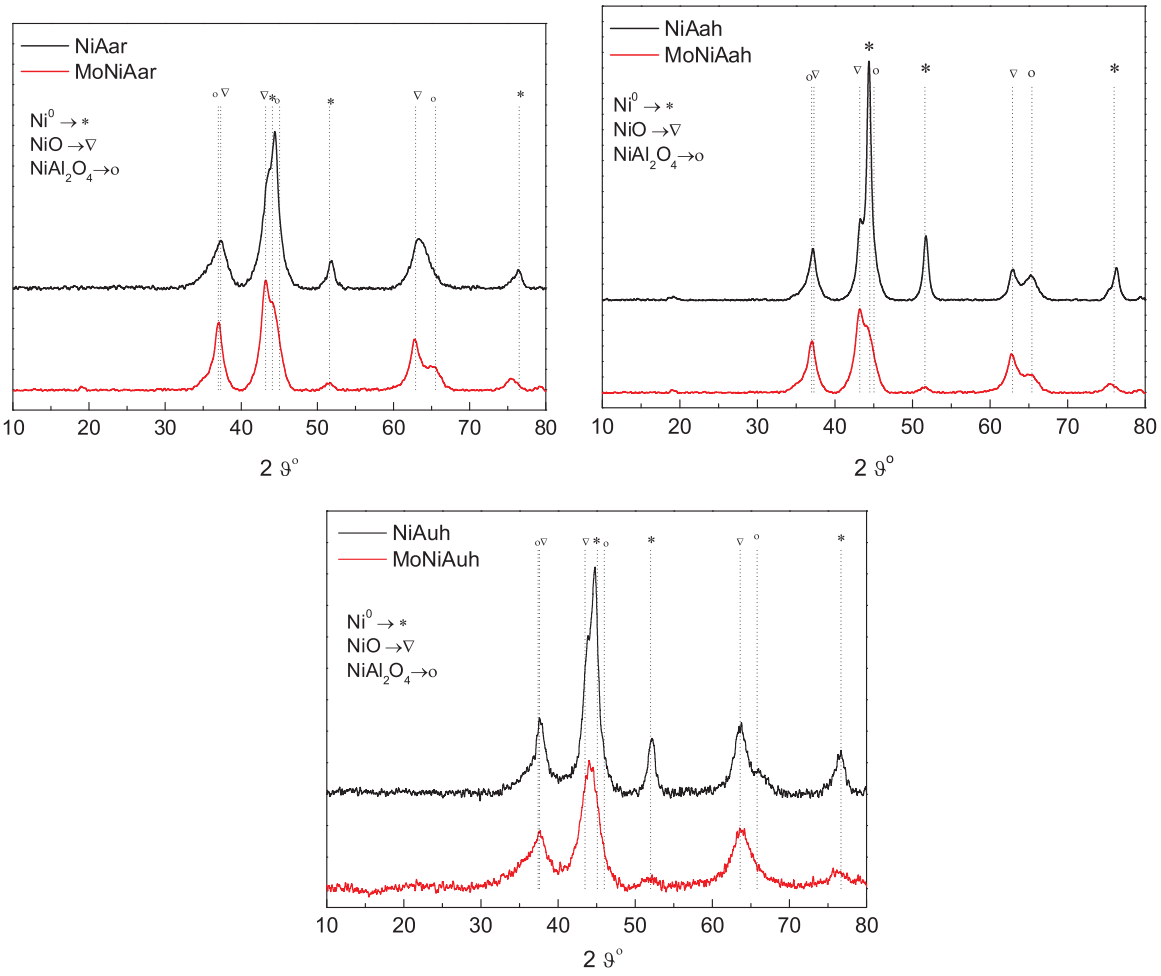

Fig. 4. XRD patterns of the NiA and MoNiA catalysts prepared by co-precipitation using NH_3 at room (ar) or high (ah) temperature and urea at high temperature (uh).

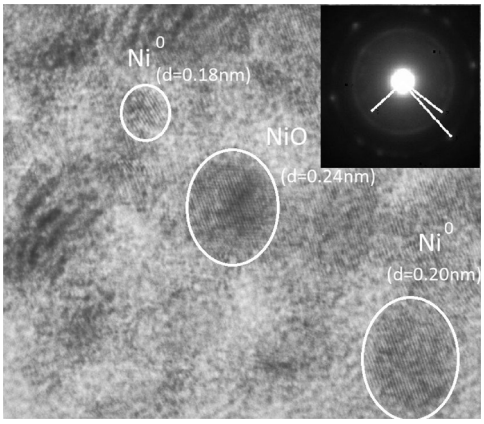

Fig. 5. HRTEM image of the sample MoNiAah. The crystal planes of metallic nickel (2 0 0/d = 0.20 nm and 2 2 0/d = 0.18 nm) and the crystal planes (1 1 1) of nickel oxides can be observed.

Moreover, the presence of these species increases considerably the reduction temperature and the magnitude of the high reduction temperature NiO peak. The increase in the reduction temperature is in line to the XPS results which showed that the presence of Mo oxo-species favors NiO with respect to Ni°. Moreover, the above observations indicate that the Mo oxo-species favor the formation of well dispersed NiO phase which are transformed into well dispersed Ni° upon reduction, in full agreement with the XRD and TEM results.

Concentrating our attention to the peak corresponding to $NiAl_2O_4$ we are observing that the presence of Mo oxo-species provokes a dramatic decrease in the amount of this catalytically inactive crystal phase. This is in good agreement to the recent literature [34].

The characterization of the samples presented so far has indicated that the Mo oxo-species are causing three effects on the nickel phases: (i) the increase in the dispersion of the metallic nickel (XRD) or the metallic nickel/nickel oxide (TEM), (ii) the resistance in the reduction of the nickel oxide (XRD, XPS, H_2-TPR) and (iii) the decrease in the amount of the nickel aluminate (XRD but mainly H_2-TPR). In the following we are attempting to provide a reasonable picture explaining these effects. Upon the co-precipitation step aluminum and the nickel hydroxides as well as precursor of $NiAl_2O_4$ like phase are formed. In the case of the presence of monomeric Mo oxo-species (Raman) they interact with the Ni^{2+} hexahydrate species provoking diminution of Ni $(OH)_2$ nanocrystals size formed increasing thus their dispersion. The aforementioned phases are dehydrated and transformed into aluminum oxide, nickel oxide and $NiAl_2O_4$ upon drying and mainly upon the step of heating in argon atmosphere. The reduction of the small NiO nanocrystals in the final activation step, though quite difficult, leads to small nickel supported nanocrystals. At the same time the aforementioned interaction between Mo oxo-species and Ni^{2+} species during co-precipitation decreases the intensity of the interaction of the latter with the alumina precursor phase diminishing the final amount of the catalytically inactive nickel aluminate formed.

The surface acidity of the samples was investigated by NH_3 desorption experiments (NH_3-TPD). NH_3 gets easily adsorbed onto the acid centers of a catalyst surface and the increase in desorption temperature

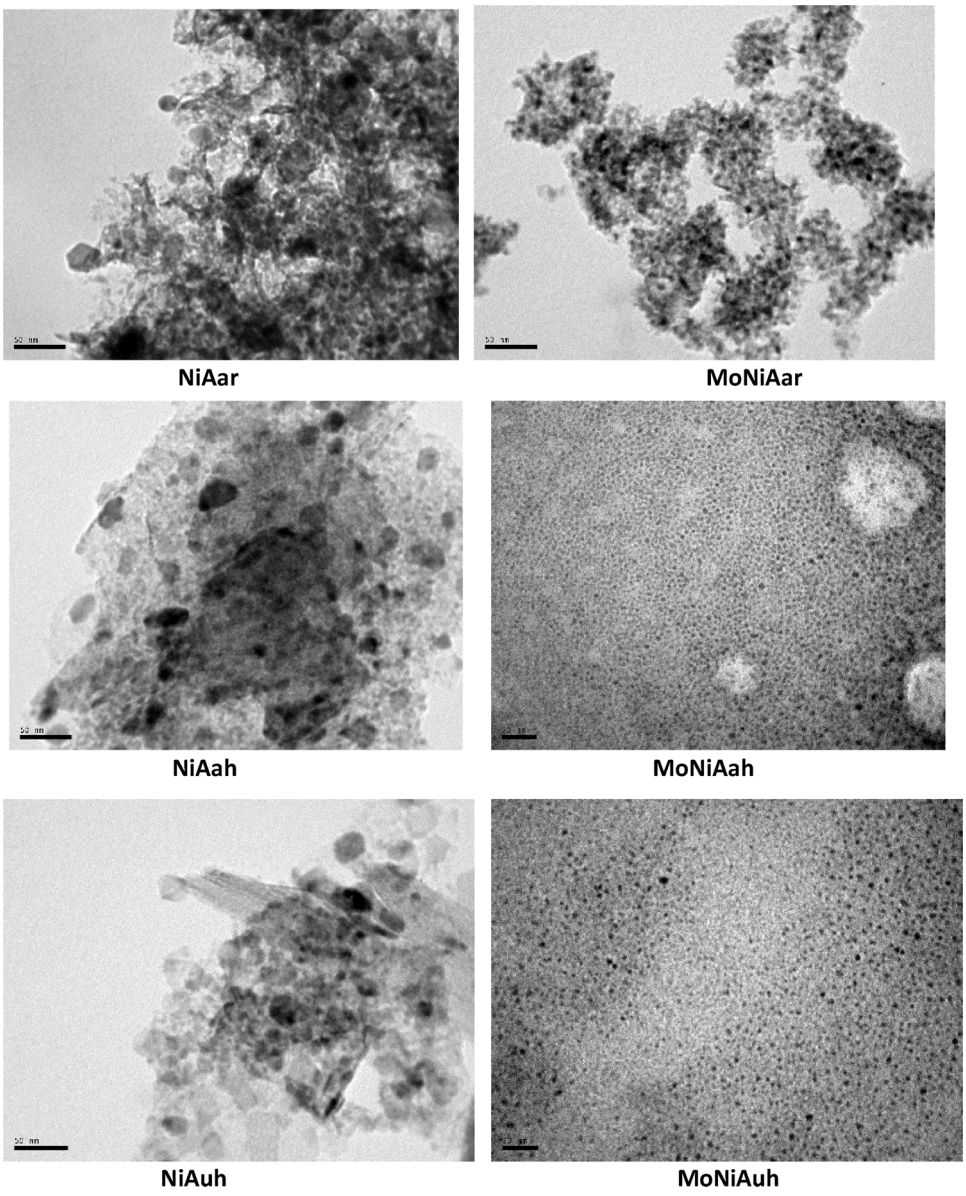

Fig. 6. TEM images of the NiA and MoNiA catalysts prepared by co-precipitation using NH_3 at room (ar) or high (ah) temperature and urea at high temperature (uh).

is directly proportional to the increase in acidity strength of the surface [64]. It has been generally accepted that the acidic sites are classified into three types: weak (desorption temperature of ammonium ions (T_{des}) < 300 °C), medium (300 °C < T_{des} < 450 °C), and strong (T_{des} > 450 °C) [65,66]. The area under the NH_3 desorption curve in the aforementioned regions can be used to calculate the quantities of acidic sites. The ammonia desorption curves of the samples studied are illustrated in Fig. 10. Inspection of this figure shows that all the unprompted samples exhibit acid sites of weak and medium strength. The population of weak acid sites seems to be about triple ($(\frac{W}{M})_{TPD}$ = 2.6−3.2) of that of the medium strength (Table 1). The addition of the molybdenum oxo-species increases considerably the total acid sites population in all studied samples, but they do not create strong ones and do not change significantly the active sites distribution (Table 1). It is important to note that the preparation method affects the magnitude of the effect of the Mo oxo-species on acid cites population. The maximum effect is observed in the sample prepared using urea aqueous solution and the less important using NH_4OH aqueous solution at high temperature (Fig. 10).

3.2. Catalysts evaluation

A representative chromatogram taken by sampling the *liquid phase* of the reactor after 1 h of reaction over MoNiAah catalyst at 310 °C and 40 bar hydrogen pressure is illustrated in Fig. 11.

One may observe peaks corresponding to n-C_{17}, n-C_{18}, n-C_{15} and n-C_{16}. Considerable amounts of alkanes with smaller number of carbon atoms were not detected indicating negligible fragmentation of the fatty acid chains. Moreover, one may observe peaks corresponding to intermediate compounds such as octadecanol, stearic acid, propyl and methyl esters, esters of fatty acids with fatty alcohols as well as unreacted triglycerides. The GC–MS analysis is in agreement with the chromatographic results. Propane, CH_4, CO, and CO_2 have been detected in the gas phase.

The detection of the above molecules is in accordance to the SDO network proposed over the nickel based catalysts [2,32] and nickel based catalysts promoted by molybdenum [34]. According to this network the normal alkanes are the only end products in the liquid phase. The other molecules are intermediate products. This is corroborated by our kinetic results. Representative kinetic results are illustrated in

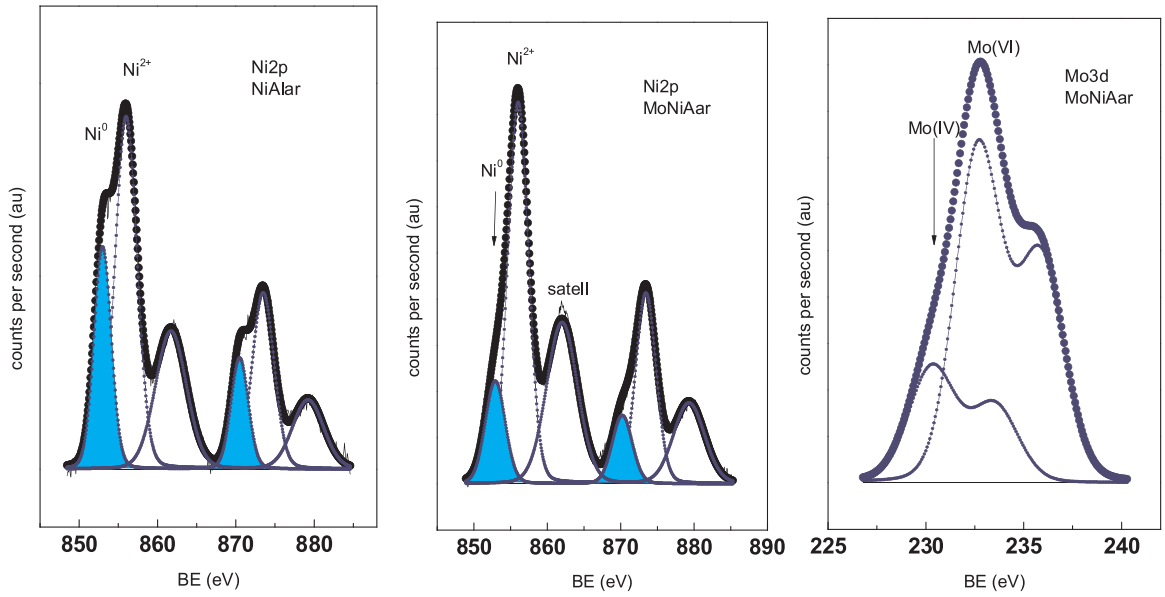

Fig. 7. Ni2p and Mo3d core level XPS spectra recorded for the samples NiAar and MoNiAar.

Table 2
Binding energies (eV) of core levels and surface atomic ratios obtained by XPS analysis of the studied catalysts.

Catalyst	$Mo3d_{5/2}$ [a]	$Ni2p_{3/2}$ [a]	$(Mo/Al)_{at}$	$(Ni/Al)_{at}$	$(\frac{Ni}{Ni+Mo})_{at}$
NiAar	–	853.0 (33)	–	0.333	–
		856.0 (67)			
NiAah	–	852.8 (42)	–	0.547	–
		855.8 (58)			
NiAuh	–	852.8 (22)	–	0.504	–
		856.3 (78)			
MoNiAar	230.3 (26)	852.9 (23)	0.060	0.427	0.877
	232.7 (74)	856.0 (77)			
MoNiAah	229.1 (40)	852.8 (39)	0.090	0.840	0.903
	232.2 (60)	855.8 (61)			
MoNiAuh	230.5 (30)	853.5 (18)	0.041	0.704	0.945
	232.9 (70)	856.4 (82)			

[a] The low BE values concern Mo(iv) (2nd column) and the Ni^0 (3rd column) whereas the high BE values refer to Mo(vi) (2nd column) and Ni^{2+}(3rd column). Values in parentheses represent the percentage of the corresponding oxidation state of the metals.

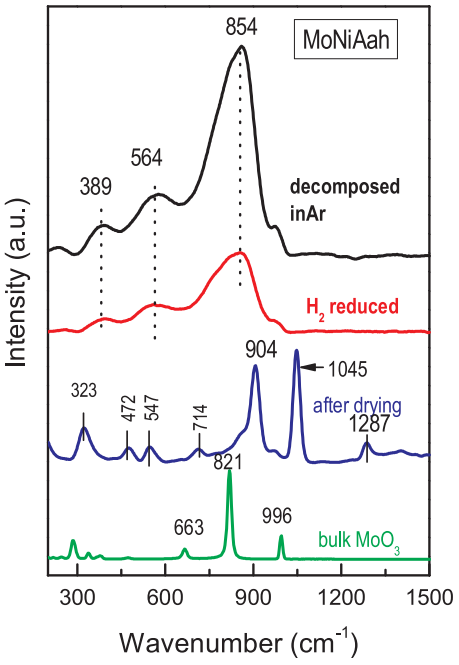

Fig. 8. Raman spectra of the sample MoNiAah recorded after each step of the preparation procedure and the spectrum of bulk MoO_3.

Fig. 12.

In fact, it is seen that the n-alkanes percentage increases monotonically with the reaction time, whereas those of the intermediate fatty acids, fatty alcohols, or esters passes through a maximum. We are noting that the percentage of the un-reacted SO or WCO decreases rapidly approaching zero achieving almost complete conversion after 3 h.

The evaluation of the catalysts after 9 h of reaction is represented in Fig. 13. Let's first concentrate our attention to the transformation of SO into green diesel (Fig. 13, left). In all cases, we are noting an increase in the hydrocarbons percentage due to the presence of the Mo species. Specifically, the hydrocarbons percentage composition in liquid product was increased by Mo addition from 47 to 66, from 24 to 97 and from 31 to 73 wt% over the ar, ah and uh catalysts, respectively. Thus, the Mo promoting action is clearly demonstrated. It is reasonable attributing this promoting action to the decrease in the size of the Ni° nanocrystals and the decrease in the amount of the catalytically inactive nickel aluminate brought about by the aforementioned Mo species.

It seems that these effects over-compensate the third effect, negative from the view point of catalysis, caused by these Mo oxo-species, namely the decrease in the extent of transformation of nickel oxide into metallic nickel upon the activation by reduction of the samples prior to their use. Presumably, this effect is not practically so important because one can imagine that *a portion* of the very small NiO nanocrystals could be transformed into very small Ni° nanocrystals upon the hydrotreatment of SO or WCO at high hydrogen pressure (40 bar) and reaction time (up to 9 h). Strong evidences for such a transformation has provided the XPS determination of the Ni/NiO ratio on molybdenum promoted $Ni/\gamma\text{-}Al_2O_3$ samples before and after their use in the SDO of SO [34].

In this point one might argue that NiO in contact to the Mo(IV) well dispersed phase would provide Ni^{2+}…Mo^{4+} sites which can be served as adsorption and SDO sites of triglycerides and related feedstocks, like in the Ni-MoS_2 catalysts. Wagenhofer et al. [67] studying the SDO kinetics of hexadecanoic acid and of intermediated compounds (hexadecanal and hexadecanol) over unsupported MoS_2, Ni-MoS_2 and Ni_3S_2 catalysts have contributed not only to the reaction mechanism (they

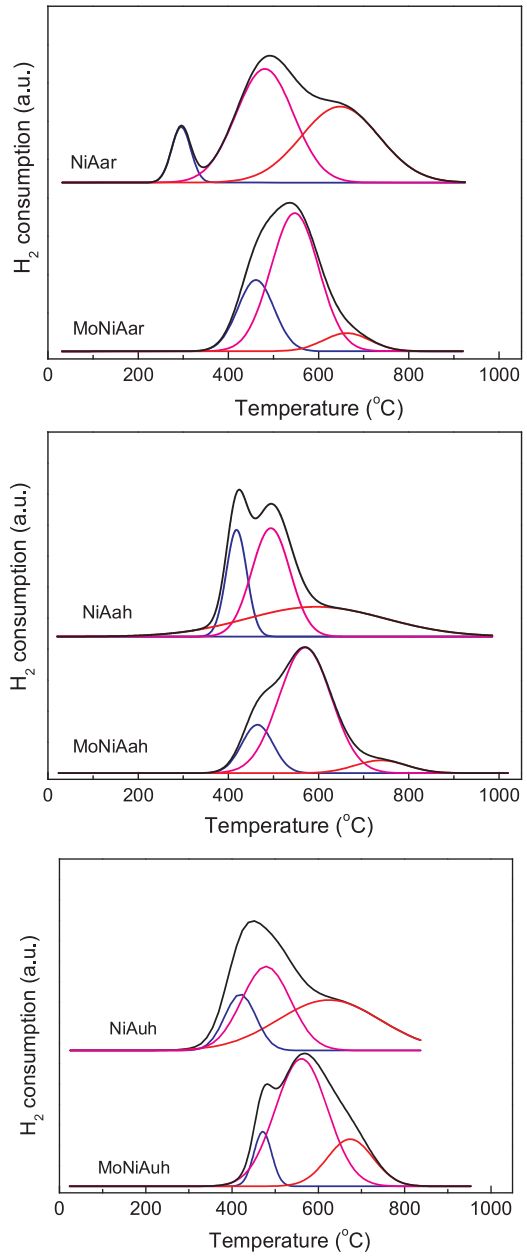

Fig. 9. H_2-TPR profiles of the NiA and MoNiA catalysts prepared by co-precipitation using NH_3 at room (ar) or high (ah) temperature and urea at high temperature (uh).

proposed decarbonylation of the hexadecanoic acid through intermediate ketene, instead of intermediate hexadecanal like in the nickel metallic catalysts) but also on the nature of active sites. They proposed a site containing 3Mo(iv), 4S(ii), 1Ni(ii) ions and one coordinately unsaturated site assigning a particular role in the S(ii) ions bonded with the Ni(ii) and in the coordinately unsaturated site. In view of the above we cannot exclude the contribution of the Ni^{2+}…Mo^{4+} like sites to decarbonylation. However, it seems to us rather marginal due to the very small amount of Mo with respect to Ni, in contrast to the catalyst composition in the aforementioned study [67]. Such a contribution would be maximized in catalysts containing more molybdenum than nickel which is not the case [34]. The high activity of the nickel metallic sites with respect of the aforementioned sites will also be inferred by the increase of the SDO performance of our MoNiah catalyst with the activation–reduction temperature which leads to the increase of the metallic nickel at expense of nickel oxide (See below in Section 3.3).

Another very interesting observation concerning the SDO of SO is that the co-precipitation mode followed affects the extent of the Mo oxo-species promoting action. The most important effect is observed in the sample prepared by co-precipitation at high temperature using ammonia as precipitating agent. The promotion obtained is indeed considerable as the composition in hydrocarbons determined after 9 h of reaction increases from 24 wt% over the un-promoted catalyst into 97 wt% over the promoted one. In fact, the chromatographic analysis of liquid phase obtained after 9 h of reaction over this promoted catalyst showed only the presence of green diesel hydrocarbons and only traces of other molecules (Fig. 14).

The highest catalytic performance exhibited by the MoNiAah catalyst can be mainly attributed to the highest dispersion of the molybdenum and nickel species achieved in this catalyst (Tables 1 and 2, Fig. 5). The second reason for this very high activity is related to acidity. Inspection of Fig. 13 (left) shows that the higher activity of the sample MoNiAah with respect to the MoNiAuh and MoNiAar ones is related to the no formation of the intermediate fatty acid-fatty alcohols big esters that undergo more difficult SDO that the natural triglycerides [2,32,34]. These are formed by reaction of the intermediate fatty acids with the intermediate fatty alcohols [2,32,34]. The high acidity favors esterification. This competes the dehydration of the fatty alcohols which results to hydrocarbons with even number of carbon atoms [35,44]. The latter reaction takes also place at moderate acidity. Inspection of Fig. 10 shows that the sample MoNiAah presents moderate acidity favoring the dehydration of the intermediate fatty alcohols with respect to their esterification. In contrast, the less active samples MoNiAar and MoNiAuh present high acidity favoring esterification. In any case the catalytic performance of the MoNiAah sample is mainly determined by the very high dispersion of the Mo and Ni species obtained over this sample and secondarily by its moderate surface acidity.

Let's now concentrate our attention to the transformation of WCO into green diesel (Fig. 13, right). Again we are noting a considerable increase in the hydrocarbons percentage in the liquid products obtained over the Mo promoted catalysts. The above considerations concerning the promoting action of the Mo oxo species are valid in general lines. However, we are noting that the highest promotion is obtained over the MoNiAar catalyst (from ~10 to 76 wt % hydrocarbons). It seems that the co-precipitation mode that should be adopted depends on the nature of the feedstock. However, it is not easy explaining why the MoNiAar catalyst is the most active among the Mo promoted ones for transformation of WCO to green diesel. A strict difference concerns their texture. Inspection of Fig. 3 shows that the volume of the relatively small mesopores in the range 3–9 nm is considerably larger in the MoNiAar catalyst ensuring higher SSA than that of the MoNiAah and MoNiAuh catalysts. Due to their configuration the diffusion of the bulky oligomers contained in WCO inside these small mesopores is quite difficult compared to that of the triglycerides and free fatty acids. Therefore, the active sites accommodated inside these pores remain available for the transformation of latter molecules into alkanes. It is recently reported that WCO contains 1.5 wt% oligomers while the SO does not [34]. Thus, the pore structure of the MoNiAar sample is more suitable for the SDO of WCO with respect to that of SO. The above is a tentative explanation for approaching a quite difficult problem required more research.

More insights concerning the promoting action of molybdenum phases can be obtained by examining the effect of these phases on the SDO network [2, 32, and 34]. Two important inter-converted intermediates are fatty aldehydes and fatty alcohols. The deCO of the former results to hydrocarbons with odd numbers of carbon atoms (mainly n-C_{15} and n-C_{17}). The HDO of the latter finally results to hydrocarbons with even numbers of carbon atoms (mainly n-C_{16} and n-C_{18}).

Inspection of Fig. 15 shows that in almost all cases the Mo promotion favors more the production of hydrocarbons with even number of carbon atoms. This indicates that the Mo promotion affects the SDO network accelerating more the HDO of the intermediate fatty alcohols. This observation is in good agreement with the literature [1–4,34].

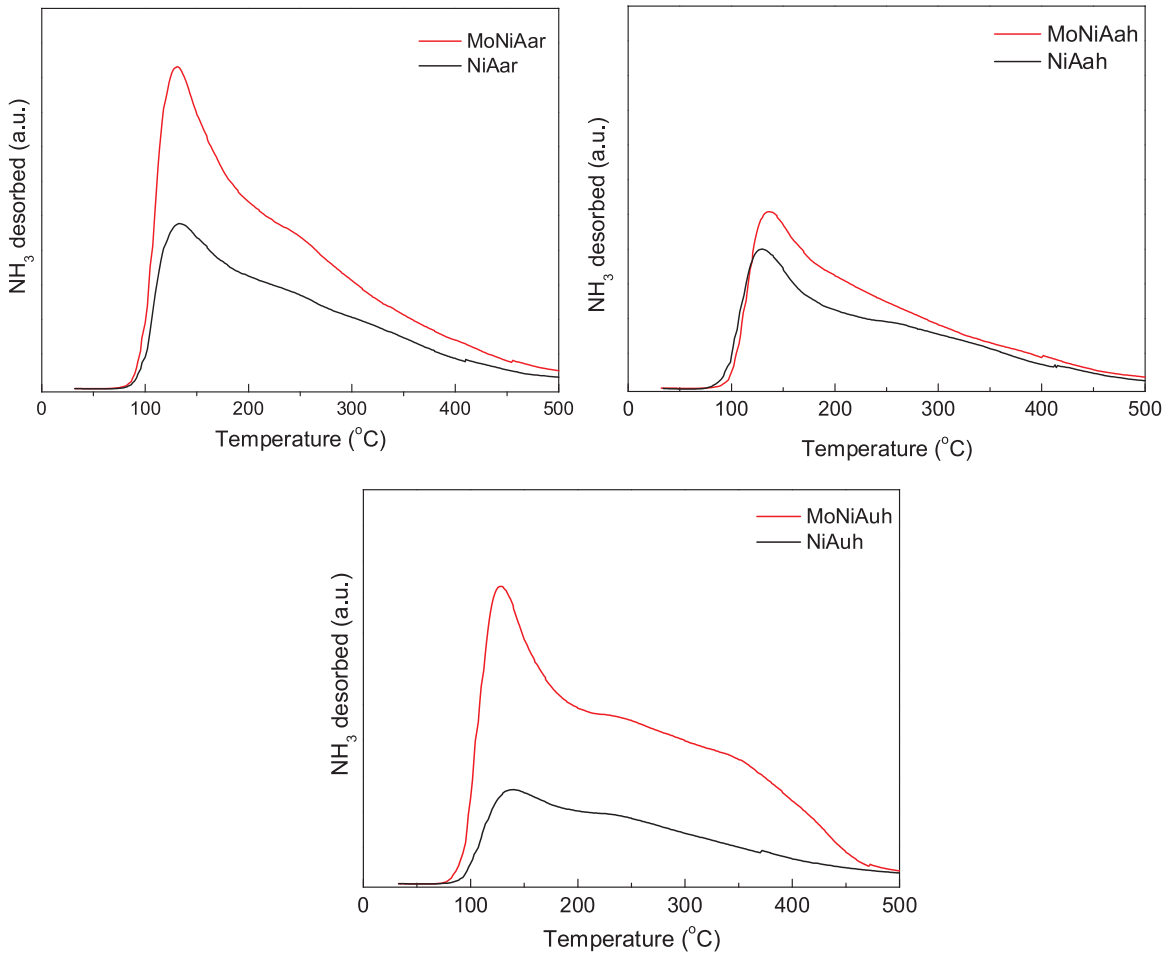

Fig. 10. Ammonia desorption profiles of the NiA and MoNiA catalysts prepared by co-precipitation using NH_3 at room (ar) or high (ah) temperature and urea at high temperature (uh).

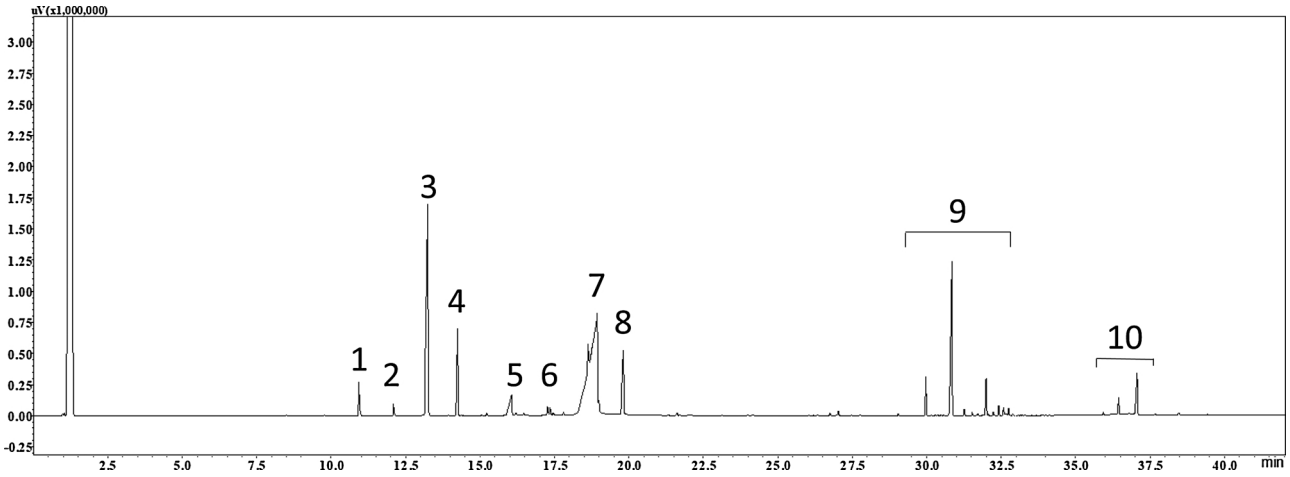

Fig. 11. GC analysis of liquid phase upon SDO of SO over MoNiAah after 1h of reaction. (1: pentadecane, 2: hexadecane, 3: heptadecane, 4: octadecane, 5: palmitic acid, 6: octadecanol, 7: stearic acid, 8: methyl-/propyl-stearic ester, 9: high molecular weight esters 10: unreacted SO).

The considerations of the preceding paragraphs of this section revealed the relation of the catalytic performance with some physicochemical properties of the catalysts studied. In contrast, one cannot observe some relation between morphology (Fig. 1) and catalytic performance (Fig. 13). This is because the aforementioned properties concern nano-scale strongly related to catalysis, for example the size of the Ni/NiO nanoparticles (Fig. 6), whereas morphology is manifested at micro-scale.

3.3. Optimization of the activation procedure-reusability (stability) of the catalysts

As already mentioned the presence of Mo oxo-species in the catalyst formulations has a negative effect, besides the positive effects discussed above, that is the inhibition of the reduction of the small NiO nanocrystals in the reduction step of the activation procedure. A plausible question is whether this can be somewhat overcome by increasing the reduction temperature of the catalysts. The study was limited to the

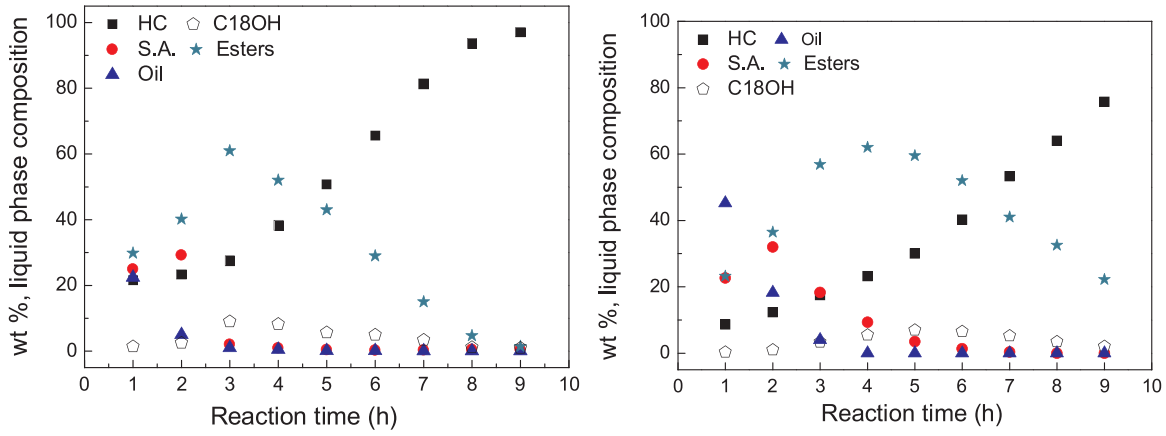

Fig. 12. Kinetics of transformation of SO over the catalyst MoNiAah (left) and WCO over the catalyst MoNiAar (riht). The composition of the liquid phase for a given time in hydrocarbons (HC), stearic acid (SA), esters of fatty acids with fatty alcohols (esters), octadecanol ($C_{18}OH$) and unreacted SO or WCO (Oil) at various times is illustrated. Reaction conditions: 100 mL Oil : 1 g $_{cat}$, 310 °C, 40 bar.

most active catalyst for the SDO of SO (MoNiAah).

Fig. 16 illustrates the composition of the liquid phase in hydrocarbons determined at various times over the most active catalyst for the SDO of SO (MoNiAah) reduced at various temperatures. One may observe that the concentration of hydrocarbons in the liquid product is increasing by increasing the reduction temperature from 400 to 500 °C and then it decreases as the reduction temperature increases from 500 to 550 °C. The concentration of oxygenated intermediates (fatty acids, fatty alcohols, and esters) was changed with reaction time following similar trends with those presented in Fig. 12 (left).

In order to rationalize the aforementioned trend concerning the effect of reduction temperature on catalytic performance we studied its influence on the textural and structural characteristics of the MoNiAah catalyst.

Inspection of Table 3 shows that the increase in the reduction temperature brings about a decrease in the specific surface area due to the shift of the pore volume distribution (not presented here) to larger pores. This is reflected to the increase of the mean pore diameter illustrated in Table 3. Obviously, the decrease in the specific surface area is negative from the catalytic point of view.

Fig. 17 illustrates the XRD patterns of the sample MoNiAah reduced at various temperatures.

It may be seen that the increase in the reduction temperature is causing an impressive increase of the extent of transformation of the NiO into Ni° nanocrystals. This is reflected to the decrease (increase) in the intensity of the peaks corresponding to NiO (Ni^0). Obviously, this effect is very positive concerning the catalytic performance as the active centers are situated on the metallic nickel. Moreover, the increase in the reduction temperature somewhat increases the amount of the catalytically inactive nickel aluminate reflected in the increase of the intensity of the peak at 2θ = 65.37°. In conclusion, the aforementioned opposite effects on the texture and structure brought about by increasing the reduction temperature explain why the maximum activity is obtained at an intermediate temperature.

The increase in the amount of the metallic nickel upon increasing the reduction temperature from 400 to 500 °C is expected increasing the catalytic performance of the MoNiAah catalyst not only for the SDO of SO but also for the SDO of WCO. This is the case as one may see by inspecting Fig. 18. In fact, the increase in the catalytic activity is actually impressive.

Finally, we are presenting our results concerning the stability and eventual reusability of the Mo promoted catalysts. Again the study was limited to the most active catalyst for the SDO of SO (MoNiAah, reduced at 500 °C). The catalyst was tested in four runs. The reaction time for each run was 9 h. After each run the liquid product was removed, the reactor was filled again with a new batch of SO and the catalytic test was repeated under the conditions described in the experimental part. The analysis of the liquid product was performed at the end of each run. After the fourth run the catalyst was analyzed for carbon deposition. The impressive catalytic result obtained after the first run over this catalyst (Fig. 13, left) was practically repeated after each of the remainder runs. Moreover, carbon analysis of the used catalyst revealed

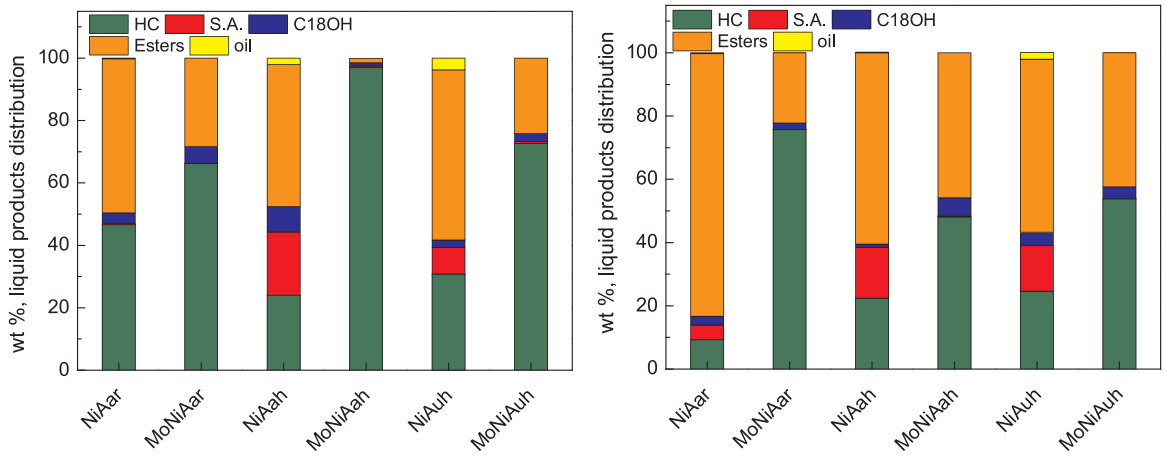

Fig. 13. Liquid products distributions obtained upon the transformation of SO (left) and WCO (right) into green diesel over the catalysts studied after 9 h of reaction at 310 °C and 40 bar H_2 pressure.

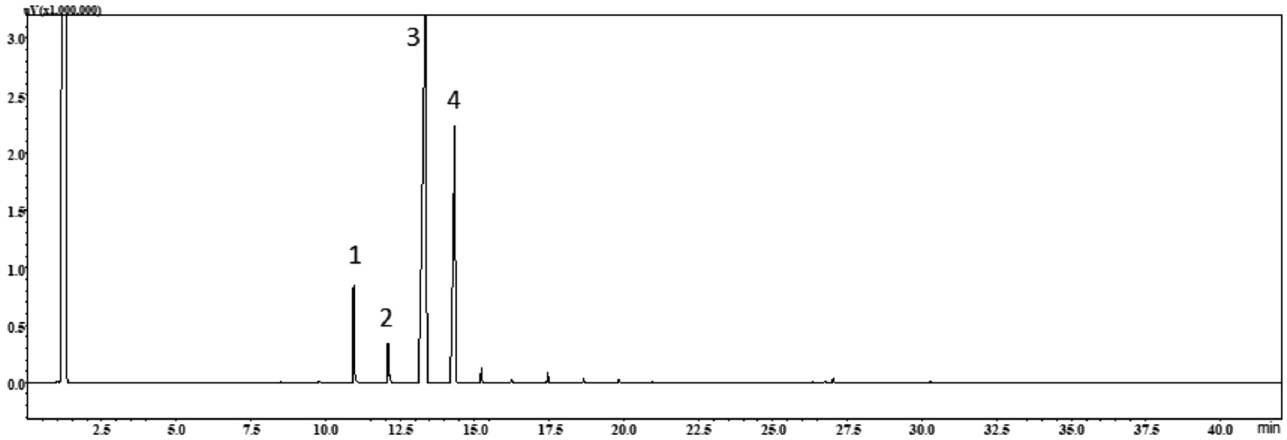

Fig. 14. GC analysis of liquid products of the SDO of SO over MoNiAah after 9 h of reaction at 310 °C and 40 bar H_2 pressure. (1: pentadecane, 2: hexadecane, 3: heptadecane, 4: octadecane).

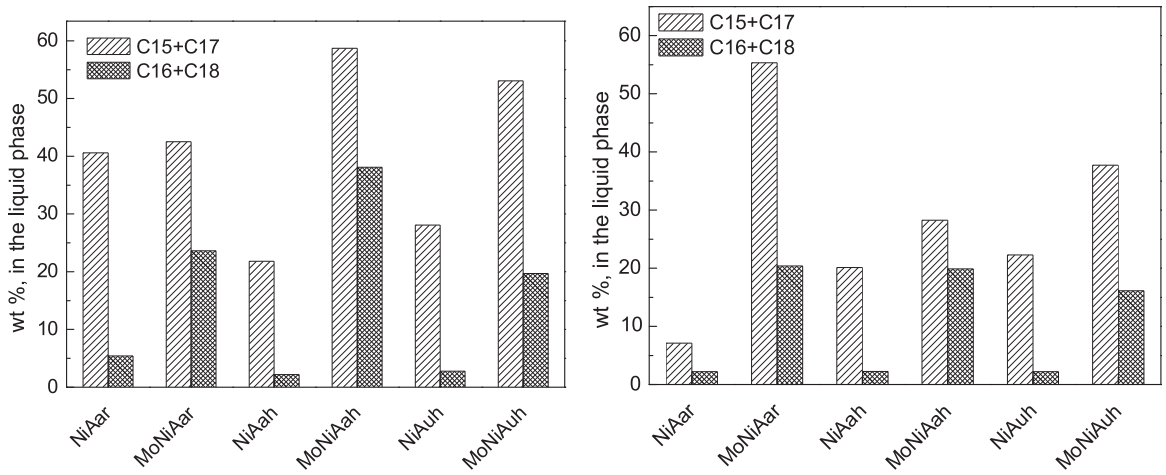

Fig. 15. Composition of the liquid product in n-alkanes with odd and even numbers of carbon atoms obtained over the catalysts studied for reaction time equal to 9 h: SDO of SO (left), SDO of WCO (right).

that carbonaceous species were not practically detected after the fourth run justifying the high catalyst stability. As our catalytic tests were performed on a semi batch reactor it seems to us interesting trying express the stability of the aforementioned catalyst in terms of the "time on the stream" usually reported for evaluation test using a fixed bed reactor. Taking into account that the total amount of SO treated in the four runs is equal to 400 mL for reaction time 36 h (corresponding to LHSV = 11.1 h^{-1}) and adopting a reasonable value for LHSV for industrial applications equal to 2 h^{-1} our experiments simulate a continuous experiment with a duration of 200 h "time on stream". The above clearly show that the most active catalyst developed in the present study is also very stable.

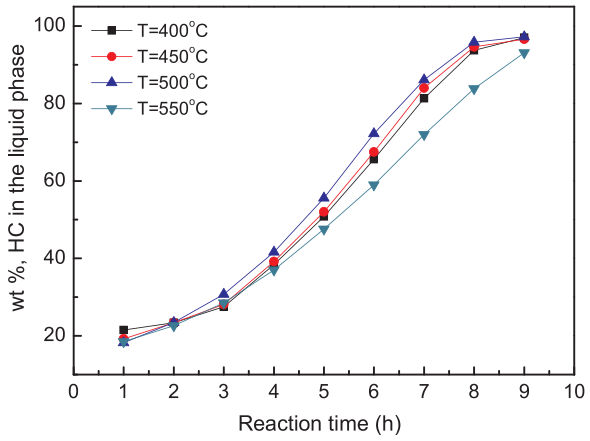

Fig. 16. The evolution with time of the composition of the liquid phase in hydrocarbons during SDO of SO over the MoNiAah catalyst reduced at various temperatures (reaction temperature: 310 °C, H_2 pressure: 40 bar, oil to catalyst ratio: 100 mL/1 g).

4. Conclusions

The various modes of the co-precipitation procedure followed for the preparation Mo-promoted Ni-Al_2O_3 catalysts with very high loading of nickel resulted to catalysts with high catalytic activity for the selective deoxygenation of sunflower oil and waste cooked oil taking into account the very high ratio of reactant volume to catalyst mass (100 mL/1 g) and that the evaluation tests were performed under solvent free conditions. The promoting action of the Mo(VI) and Mo(IV) well dispersed oxo-species, present in these catalysts, was demonstrated in all cases. This promoting action was attributed to the impressive decrease in the size of the supported nickel nanoparticles and the inhibition of the formation of the catalytically inactive nickel aluminate. In addition, the presence of the Mo(VI) and Mo(IV) oxo-species affect the selective deoxygenation network favoring more the hydrodeoxygenation of the intermediate alcohols with respect to the decarbonylation of intermediate aldehydes.

The more suitable mode of the co-precipitation procedure that should be followed depends on the oil to be transformed into green

Table 3
Textural parameters of the MoNiAah catalyst activated at various temperatures by reduction.

Reduction Temperature (°C)	SSA (m^2/g)	SPV (cm^3/g)	MPD (nm)
400	219	0.53	9.4
450	194	0.53	10
500	169	0.54	11.7
550	140	0.56	13.7

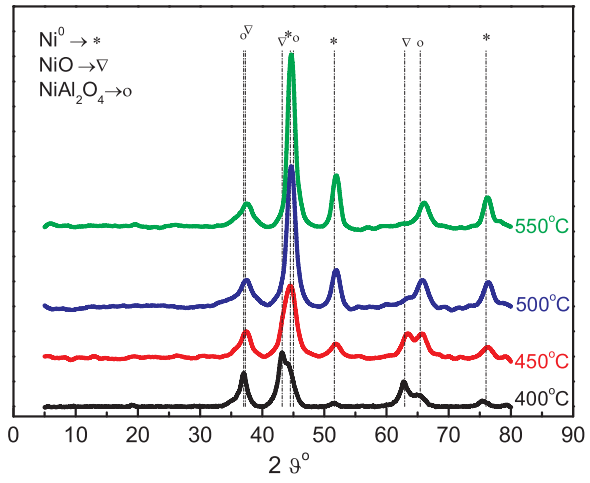

Fig. 17. XRD patterns of the sample MoNiAah reduced at various temperatures.

diesel. The catalyst prepared at high co-precipitation temperature using ammonia as precipitating agent (MoNiAah) was proved to be the most active for the selective deoxygenation of sunflower oil. An almost complete transformation of it into n-C_{15}, n-C_{16}, n-C_{17}, n-C_{18} (green diesel) was obtained at 310 °C, hydrogen pressure 40 bar and reactant volume to catalyst mass ratio equal to 100 mL/1 g working under solvent free conditions. The catalytic activity of this catalyst was further increased by increasing its reduction temperature from 400 to 500 °C in the context of activation procedure. This catalyst was proved to be very stable as its activity was kept practically constant for, at least, four runs. The catalyst prepared at room co-precipitation temperature using ammonia as precipitating agent (MoNiAar) was proved to be the most active for the selective deoxygenation of waste cooked oil. Its higher activity with respect to the other Mo promoted catalysts was related to the high population of small mesopores of 2–9 nm which can preclude oligomers contained in this feedstock from the active sites being on the surface inside these pores remaining thus available for the transformation of free fatty acids and triglycerides into green diesel.

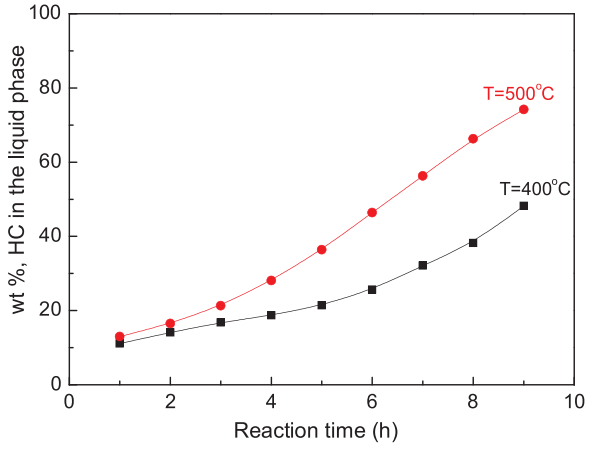

Fig. 18. The evolution with time of the composition of the liquid phase in hydrocarbons during the SDO of WCO over the MoNiAah catalyst reduced at 400 (■) and 500 °C (●).

Acknowledgments

Financial support of the present work from the "RESEARCH PROJECTS FOR EXCELLENCE IKY/SIEMENS" program is gratefully acknowledged. We also acknowledge the contribution of Dr. A. Seferlis for SEM–EDX analysis, Dr. M. Kollia for TEM analysis of the catalysts at the laboratory of Electron Microscopy and Microanalysis of the University of Patras and Mr. M. Kourtelesis for NH_3-TPD experiments.

References

[1] I. Kubickova, D. Kubicka, Waste Biomass Valoriz. 1 (2010) 293–308.
[2] C. Kordulis, K. Bourikas, M. Gousi, E. Kordouli, A. Lycourghiotis, Appl. Catal. B 181 (2016) 156–196.
[3] C. Zhao, T. Brück, J.A. Lercher, Green Chem. 15 (2013) 1720–1739.
[4] R.W. Gosselink, S.A.W. Hollak, S.-W. Chang, J. van Haveren, K.P. de Jong, J.H. Bitter, D.S. van Es, ChemSusChem 6 (2013) 1576–1594.
[5] S. Karatzos, J.S. van Dyk, J.D. McMillan, J. Saddler, Biofuels Bioprod. Bioref. 11 (2017) 344–362.
[6] P. Suwannasom, P. Kham-or, C. Ruangviriyachai, Energy Source Part A 38 (2016) 3549–3556.
[7] P. Kham-or, P. Suwannasom, C. Ruangviriyachai, Energy Source Part A 38 (2016) 3694–3701.
[8] Q. Zheng, L. Huo, H. Li, S. Mi, X. Li, X. Zhu, X. Deng, B. Shen, Fuel 202 (2017) 563–571.
[9] M.V. Domínguez-Barroso, C. Herrera, M.A. Larrubia, L.J. Alemany, Fuel Proc. Technol. 148 (2016) 110–116.
[10] L. Zhou, A. Lawal, Catal. Sci. Technol. 6 (2016) 1442–1454.
[11] M.R. Nimkarde, P.D. Vaidya, Energy Fuels 30 (2016) 3107–3112.
[12] N. Chen, N. Wang, Y. Ren, H. Tominaga, E.K. Qian, J. Catal. 345 (2017) 124–134.
[13] H. Chen, X. Zhang, Q. Wang, Catal. Commun. 97 (2017) 14–17.
[14] R. Kumar, S.A. Farooqui, M. Anand, R. Kumar, R. Joshi, A. Khan, A.K. Sinha, Catal. Commun. 98 (2017) 102–106.
[15] N. Luo, Y. Cao, J. Li, W. Guo, Z. Zhao, J. Fuel Chem. Technol. 44 (2016) 76–83.
[16] C. Liu, H. Yang, Z. Jing, K. Xi, C. Qiao, J. Fuel Chem. Technol. 44 (2016) 1211–1216.
[17] S. Zhao, Z. Zhang, K. Zhu, J. Chen, Appl. Surf. Sci. 404 (2017) 388–397.
[18] H. Chen, Y. Wu, S. Qi, Y. Chen, M. Yang, Appl. Catal. A 529 (2017) 79–90.
[19] Y. Cao, Y. Shi, J. Liang, Y. Wu, S. Huang, J. Wang, M. Yang, H. Hu, Chem. Eng. Sci. 158 (2017) 188–195.
[20] Y. Shi, E. Xing, Y. Cao, M. Liu, K. Wu, M. Yang, Y. Wu, Chem. Eng. Sci. 166 (2017) 262–273.
[21] N. Arun, J. Maley, N. Chen, R. Sammynaiken, Y. Hu, A.K. Dalai, Catal. Today 291 (2017) 153–159.
[22] E. Baldauf, A. Sievers, T. Willner, Biofuels 8 (2017) 555–564.
[23] M. Ameen, M.T. Azizan, S. Yusup, A. Ramli, M. Yasir, Renew. Sustain. Energy Rev. 80 (2017) 1072–1088.
[24] H.S.H. Nguyen, P. Mäki-Arvela, U. Akhmetzyanova, Z. Tišler, I. Hachemi, A. Rudnäs, A. Smeds, K. Eränen, A. Aho, N. Kumar, J. Hemming, M. Peurla, D.Y. Murzin, J. Chem. Technol. Biotechnol. 92 (2017) 741–748.
[25] M. Peroni, I. Lee, X. Huang, E. Barath, O.Y. Gutiérrez, J.A. Lercher, ACS Catal. 7 (2017) 6331–6341.
[26] K. Jenišťová, I. Hachemi, P. Mäki-Arvela, N. Kumar, M. Peurla, L. Capek, J. Wärnå, D.Y. Murzin, Chem. Eng. J. 316 (2017) 401–409.
[27] M. Yasir, M. Tazli Azizan, A. Ramli, M. Ameen, Proc. Eng. 148 (2016) 275–281.
[28] H. Xin, K. Guo, D. Li, H. Yang, C. Hu, Appl. Catal. B 187 (2016) 375–385.
[29] I. Hachemi, K. Jenistova, P. Mäki-Arvela, N. Kumar, K. Eränen, J. Hemming, D. Murzin, Catal. Sci. Technol. 6 (2016) 1476–1487.
[30] P. Munnik, P.E. de Jongh, K.P. de Jong, Chem. Rev. 115 (2015) 6687–6718.
[31] M. Behrens, Catal. Today 246 (2015) 46–54.
[32] M. Gousi, C. Andriopoulou, K. Bourikas, S. Ladas, M. Sotiriou, C. Kordulis, A. Lycourghiotis, Appl. Catal. A 536 (2017) 45–66.
[33] T. Kimura, H. Imai, X. Li, K. Sakashita, S. Asaoka, S.S. Al-Khattaf, Catal. Lett. 143 (2013) 1175–1181.
[34] E. Kordouli, L. Sygellou, C. Kordulis, K. Bourikas, A. Lycourghiotis, Appl. Catal. B 209 (2017) 12–22.
[35] H. Imai, T. Kimura, K. Terasaka, X. Li, K. Sakashita, S. Asaoka, S.S. Al-Khattaf, Catal. Today (2017), http://dx.doi.org/10.1016/j.cattod.2017.08.023.
[36] E. Kordouli, C. Kordulis, A. Lycourghiotis, R. Cole, P.T. Vasudevan, B. Pawelec, J.L.G. Fierro, Mol. Catal. J. 441 (2017) 209–220.
[37] J. Liu, C. Liu, G. Zhou, S. Shen, L. Rong, Green Chem. 14 (2012) 2499–2505.
[38] J. Liu, S. Yoda, J. He, L. Deng, K. Fan, L. Rong, Chem. Lett. 43 (2014) 310–312.
[39] J. Liu, K. Fan, W. Tian, C. Liu, L. Rong, Int. J. Hydrogen Energy 37 (2012) 17731–17737.
[40] C. Liu, J. Liu, G. Zhou, W. Tian, L. Rong, J. Taiwan Inst. Chem. Eng. 44 (2013) 221–227.
[41] C. Liu, J. Liu, G. Zhou, W. Tian, L. Rong, Environ. Prog. Sustain. 32 (2013) 1240–1246.

[42] K. Fan, J. Liu, X. Yang, L. Rong, Int. J. Hydrogen Energy 39 (2014) 3690–3697.
[43] X. Zhao, L. Wei, S. Cheng, J. Julson, G. Anderson, K. Muthukumarappan, C. Qiu, J. Renew. Sustain. Energy 8 (2016) 013109, http://dx.doi.org/10.1063/1.4941911.
[44] A.B. Chhetri, K. Chris Watts, M. Rafiqul Islam, Energies 1 (2008) 3–18.
[45] P.B. Weisz, W.O. Haag, P.G. Rodewald, Science 206 (1979) 57–58.
[46] G. Knothe, Prog. Energy Combust. Sci. 36 (2010) 364–373.
[47] S.B. Glisic, J.M. Pajnik, A.M. Orlovic, Appl. Energy 170 (2016) 176–185.
[48] C. Yin, L. Zhao, Z. Bai, H. Liu, Y. Liu, C. Liu, Fuel 107 (2013) 873–878.
[49] Z. Marczenko, C.G. Ransay (Ed.), Spectrophotometric Determination of Elements, Wiley, New York, 1970, p. p. 569.
[50] F.D. Snell, Photometric and Fluorometric Methods of Analysis of Metals vol. 2, Wiley, New York, 1978, p. p. 1296.
[51] N. Spanos, H.K. Matralis, C. Kordulis, A. Lycourghiotis, J. Catal. 136 (1992) 432–445.
[52] R. Miao, X. Yu, W. Zeng, Mater. Lett. 173 (2016) 107–110.
[53] R. Miao, W. Zeng, Q. Gao, Appl. Surf. Sci. 384 (2016) 304–310.
[54] J. Wang, W. Zeng, Z. Wang, Ceram. Int. 42 (2016) 4567–4573.
[55] X. Liu, X. Wang, X. Yuan, W. Dong, F. Huang, J. Mater. Chem. A 4 (2016) 167–172.
[56] E.L. Lee, I.E. Wachs, J. Phys. Chem. C 111 (2007) 1410–14425.
[57] J. Gao, Y. Zheng, J.-M. Jehng, I.E. Wachs, S.G. Podkolzin, Science 348 (6235) (2015) 686–690.
[58] S. Chempath, Y. Zhang, A.T. Bell, J. Phys. Chem. C 111 (2007) 1291–1298.
[59] A. Guevara-Lara, R. Bacaud, M. Vrinat, Appl. Catal. A 328 (2007) 99–108.
[60] G. Deo, I.E. Wachs, J. Phys. Chem. 95 (1991) 5889–5895.
[61] N. Spanos, L. Vordonis, C. Kordulis, A. Lycourghiotis, J. Catal. 124 (1990) 301–314.
[62] A. Tribalis, G.D. Panagiotou, K. Bourikas, L. Sygellou, S. Kennou, S. Ladas, A. Lycourghiotis, C. Kordulis, Catalysts 6 (2016) 11.
[63] J. Vakros, A. Lycourghiotis, G.A. Voyiatzis, A. Siokou, C. Kordulis, Appl. Catal. B 96 (2010) 496–507.
[64] M. Lewandowski, Z. Sarbak, Fuel 79 (2000) 487–495.
[65] J. Grzechowiak, J. Rynkowski, I. Wereszczako-Zielinska, Catal. Today 65 (2001) 225–231.
[66] D. Zhang, W.-Q. Liu, Y.-A. Liu, U.J. Etim, X.-M. Liu, Z.-F. Yan, Chem. Eng. J. 330 (2017) 706–717.
[67] M.F. Wagenhofer, E. Baráth, O.Y. Gutiérrez, J.A. Lercher, ACS Catal. 7 (2017) 1068–1076.